

ABSTRACT

MAKTHAL, SAMEER. Investigating Data Driven Approaches to Analyze Patient Handling of Eye-Drop Bottles. (Under the direction of Dr. Landon Grace)

Glaucoma is the leading cause of irreversible blindness and projected to affect over 100 million across the world by 2040. It is widely understood that glaucoma is caused by the death of retinal ganglion cells, but a lack of understanding of its etiology, and the patient burden associated with daily topical medication for the pharmacological reduction of intraocular pressure (IOP) makes it difficult to diagnose and manage post-diagnosis. This dissertation contributes to the management of glaucoma post-diagnosis through the evaluation of use-inspired strategies that leverage data for identifying and managing this disease effectively.

A rise in IOP is often suggested as the primary cause of glaucoma and is currently the only factor that can be modified for the treatment of this disease. A reduction in IOP can be achieved through the regular application of eye-drops and monitoring the adherence of patients to their treatment plans. Due to glaucoma being highly prevalent in the older population, adherence to regular application of eyedrops remains a major point of concern. Therefore, this body of work focuses on data-driven strategies based on the behavior associated with patient handling of eye-drop bottles for the effective management of glaucoma post-diagnosis. A deep learning approach to human activity recognition is opted to develop a model with the ability to understand patient behavior associated with adherence to glaucoma medication. Accepting the variety in scenarios associated with eyedrop medication, multiple models were developed to better explore the effectiveness of data and patient behavior for the management of this disease.

Three unique scenarios were modeled using long short-term memory (LSTM) recurrent neural networks (RNN). Scenario 'A' involved the use of a drop delivery aid called GentleDrop™ to help patients in administering a drop. A model was trained to successfully

predict the all involved activities based on inertial data recorded from volunteer interaction with eye-drop bottles. Scenario 'B' addressed the limitation of HAR models to predict the same activities recorded at different sensor orientations. Model 'B' was trained on datasets with transformed coordinates added as an additional feature. Scenario 'C' involved developing a human activity recognition model without a drop delivery aid and using a force sensitive resistor to detect handling force. Model 'A' displayed good performance in predicting the action of administering a drop. Model 'B' performance was on par with model 1 with specificity percentages over 80%. The performance of model 'C' was better in comparison, exhibiting high precision and specificity percentages. The three models showed good overall accuracy of 88%, 88% and 89% respectively.

The use of such models could have a positive impact on identifying the barriers associated with passive attitude towards topical medications. In the future, data driven models could also be integrated with the care provider management ecosystem to actively improve patient adherence to glaucoma treatment plans by intervening when medication usage wanes.

© Copyright 2023 by Sameer Makthal

All Rights Reserved

Investigating Data Driven Approaches to Analyze Patient Handling of Eye-Drop Bottles

by
Sameer Makthal

A thesis submitted to the Graduate Faculty of
North Carolina State University
in partial fulfillment of the
requirements for the degree of
Master of Science

Mechanical Engineering

Raleigh, North Carolina
2023

APPROVED BY:

Dr. Landon Grace
Committee Chair

Dr. Kara Peters

Dr. Mark Pankow

DEDICATION

This thesis is dedicated to my parents and my partner. Without their patience, sacrifice, unwavering support and most of all love, the completion of this work would not have been possible.

BIOGRAPHY

Sameer Makthal was born in Mumbai, India and spent most of his younger years growing up in Hyderabad, India. He received his bachelor's in mechanical engineering from Sreenidhi Institute of Science and Technology, an affiliate of Jawaharlal Nehru Technological University Hyderabad. Spending most of his undergraduate years building race cars and competing in SAE national championships, he built great interest in the field of design. In 2021, he decided to get his master's in mechanical engineering and joined North Carolina State University. With exposure to new fields of research and industry demands he ventured into diverse fields and joined Dr. Landon Grace and his research team in the Composite Response and Characterization Lab to explore his interests in utilizing data driven techniques to aid the medical field.

ACKNOWLEDGMENTS

I'm grateful to Dr. Landon Grace for giving me the opportunity to work in the Composite Response and Characterization (CRAC) lab and explore my research interests in the field of composite materials, design, and machine learning. I appreciate your advice and confidence in me despite circumstances. I'm grateful for my colleagues in the CRAC lab and the assistance they've provided me with over the course of my research. To my friends and family, I thank you for the support and advice you've given me throughout all the tight deadlines and roadblocks.

TABLE OF CONTENTS

| | |
|--|-----|
| LIST OF TABLES | vi |
| LIST OF FIGURES | vii |
| Chapter 1: Introduction | 1 |
| 1.1 Pathophysiology of Glaucoma | 1 |
| 1.2 Glaucoma diagnosis, treatment, and management..... | 4 |
| 1.2.1 Treatment | 4 |
| 1.3 Role of Artificial Intelligence | 6 |
| 1.4 Objectives and an overview | 6 |
| Chapter 2: Developing a Human Activity Recognition Model trained on data recorded from patient handling of eye-drop bottles. | 9 |
| 2.1 Introduction..... | 9 |
| 2.2 Method | 12 |
| 2.2.1 Prototype Hardware | 12 |
| 2.2.2 Data Collection | 14 |
| 2.3 Data preprocessing..... | 18 |
| 2.4 Model | 19 |
| 2.5 Results..... | 24 |
| 2.6 Discussion | 27 |
| Chapter 3: Investigating the effect of data coordinate transformation on HAR model trained on patient handling of eye-drop bottles. | 30 |
| 3.1 Development of transformations for alternate sensor hardware orientation..... | 30 |
| 3.1.1 An example of transformation of collected inertial data. | 34 |
| 3.2 HAR model developed on transformed accelerometer data as an added feature. | 36 |
| 3.2.1 Discussion | 40 |
| Chapter 4: Developing a HAR model trained on data with added correlating feature in the absence of GentleDrop™. | 42 |
| 4.1 Method | 42 |
| 4.1.2 Prototype Hardware | 43 |
| 4.1.3 Data Collection | 44 |
| 4.2 Model | 46 |
| 4.3 Results..... | 49 |
| 4.3.1 Comparing results. | 50 |
| 4.4 Discussion | 53 |
| Chapter 5: Conclusion | 55 |
| References | 57 |

LIST OF TABLES

| | | |
|-----------|---|----|
| Table 2.1 | Activity - specific performance metrics for the model trained on all eight activities with the use of GentleDrop™..... | 25 |
| Table 2.2 | Activity - specific performance metrics for the model trained on seven activities and the combined label 'LC' with the use of GentleDrop™. | 26 |
| Table 3.1 | Activity - specific performance metrics for the model trained transformed sensor data added as a feature..... | 40 |
| Table 4.1 | Activity - specific performance metrics for the model trained on data with FSR values as a correlating feature | 50 |
| Table 4.2 | Table 2: Activity - specific performance metrics for the model trained on data with FSR values as a correlating feature using the CNN model | 51 |

LIST OF FIGURES

| | | |
|-------------|---|----|
| Figure 1.1 | Aqueous humor drainage pathways of healthy eyes | 2 |
| Figure 1.2 | Overview of the chapters in the dissertation | 8 |
| Figure 2.1 | 3D printed holder designed to house the IMU and prototype | 13 |
| Figure 2.2 | The entire assembly with the prototype, the IMU, 3D printed holder and GentleDrop™. A screengrab of a mobile application that shows the inertial readings. | 14 |
| Figure 2.3 | The change in model overall accuracy as the training dataset is increased..... | 16 |
| Figure 2.4 | The change in acceleration and gyroscope values in each of the cartesian coordinates as the bottle is initially at rest (A), then the bottle is inserted into the GentleDrop™ (B), followed by opening the cap (C) and lifting the bottle (D) to the bridge of the nose and squeezing the bottle (E). The bottle is then lowered (F) and the cap is closed (G) before separating the bottle and GentleDrop™ (H) | 17 |
| Figure 2.5 | Data segmented into windows with an overlap to avoid transitional issues | 19 |
| Figure 2.6 | Distribution of each activity across the dataset | 20 |
| Figure 2.7 | The long short-term memory recurrent neural network architecture used for the first model | 22 |
| Figure 2.8 | The long short-term memory recurrent neural network architecture used for the second model with combined classes | 23 |
| Figure 2.9 | The confusion matrix from the model trained on all eight activities with the use of GentleDrop™ | 24 |
| Figure 2.10 | The confusion matrix from the model trained on 7 activities and the combined label LC with the use of GentleDrop™ | 26 |
| Figure 3.1 | ECEF and NED Frames with a description of each axis and its direction | 31 |
| Figure 3.2 | Orientation of Axes of Sensitivity and Polarity of Rotation for Accelerometer and Gyroscope..... | 32 |
| Figure 3.3 | The change in acceleration and gyroscope values in each of the cartesian coordinates as the bottle is initially at rest (A), then the bottle is inserted into the GentleDrop™ (B), followed by opening the cap (C) and lifting the bottle (D) to the bridge of the nose and squeezing the bottle (E). The bottle is then lowered (F) and the cap is closed (G) before separating the bottle and GentleDrop™ (H) | 35 |

| | | |
|-------------|--|----|
| Figure 3.4 | The long short-term memory recurrent neural network architecture used for the model trained on transformed sensor data as a feature | 38 |
| Figure 3.5 | The combined confusion matrix of the model trained on transformed sensor data added as a feature | 39 |
| Figure 4.1 | (A) The force sensitive resistor is made by sandwiching the velostat between two layers of faraday. (B) The FSR wrapped around the bottle..... | 44 |
| Figure 4.2 | The prototype that integrates the FSR and accelerometer data assembled with the bottle | 44 |
| Figure 4.3 | The behavior of FSR, and acceleration as each activity was performed over time.. | 45 |
| Figure 4.4 | Distribution of each activity class in the dataset | 46 |
| Figure 4.5 | The long short-term memory recurrent neural network architecture used for the model trained on sensor data integrated with FSR values..... | 48 |
| Figure 4.6 | Confusion matrix from the model trained on data with FSR values as a correlating feature | 49 |
| Figure 4.7 | Confusion matrix from the CNN model..... | 51 |
| Figure 4.8 | Comparing recall metrics per activity between LSTM and CNN model | 52 |
| Figure 4.9 | Comparing specificity metrics per activity between LSTM and CNN model | 52 |
| Figure 4.10 | Comparing precision metrics per activity between LSTM and CNN model | 53 |

CHAPTER 1

As of the turn of the century, glaucoma is now the second most common cause of blindness worldwide (1). In contrast to cataracts, which are the main cause of loss of eyesight, blindness caused by glaucoma is irreversible. Damage is caused to the optic nerve due to the accumulation of fluids and abnormality in the drainage of these fluids (2). Accumulation of fluids leads to an increase in intraocular pressure (IOP) which is strongly correlated to the death of retinal ganglion cells (3). Although IOP does not cause glaucoma in every afflicted individual, it is presently the primary controllable risk factor for glaucoma management (4). The first chapter presents an overview of the anatomy of the eye from the standpoint of glaucoma development, the currently recognized pathophysiology, illness diagnosis, therapy and management options, and a synopsis of the subsequent chapters.

1.1 Pathophysiology of Glaucoma

The pathophysiology of glaucoma is still not well understood with constant debate on whether the location of primary damage is the death of ganglion cell bodies or their axons. Irrespective of the site of neuronal injury the terminal outcome is the death of RGCs and their axons leading to irreversible vision loss (5).

Glaucoma is a heterogeneous group of diseases with various theories pointing towards factors such as elevated intraocular pressure (IOP) and vascular dysregulation contributing to primary insult. This damage is caused to glaucomatous atrophy in the form of obstruction to axoplasmic flow within the RGC axons at the lamina cribrosa, altered optic nerve microcirculation at the level of lamina and changed in the laminar glial and connective tissue. Factors such as excitotoxic damage caused by glutamate or glycine released from injured neurons and oxidative damage caused by overproduction of nitric oxide (NO) and reactive

oxygen species lead to secondary insult. The complex interplay of these factors leads to the death of RGCs and irreversible visual loss (6).

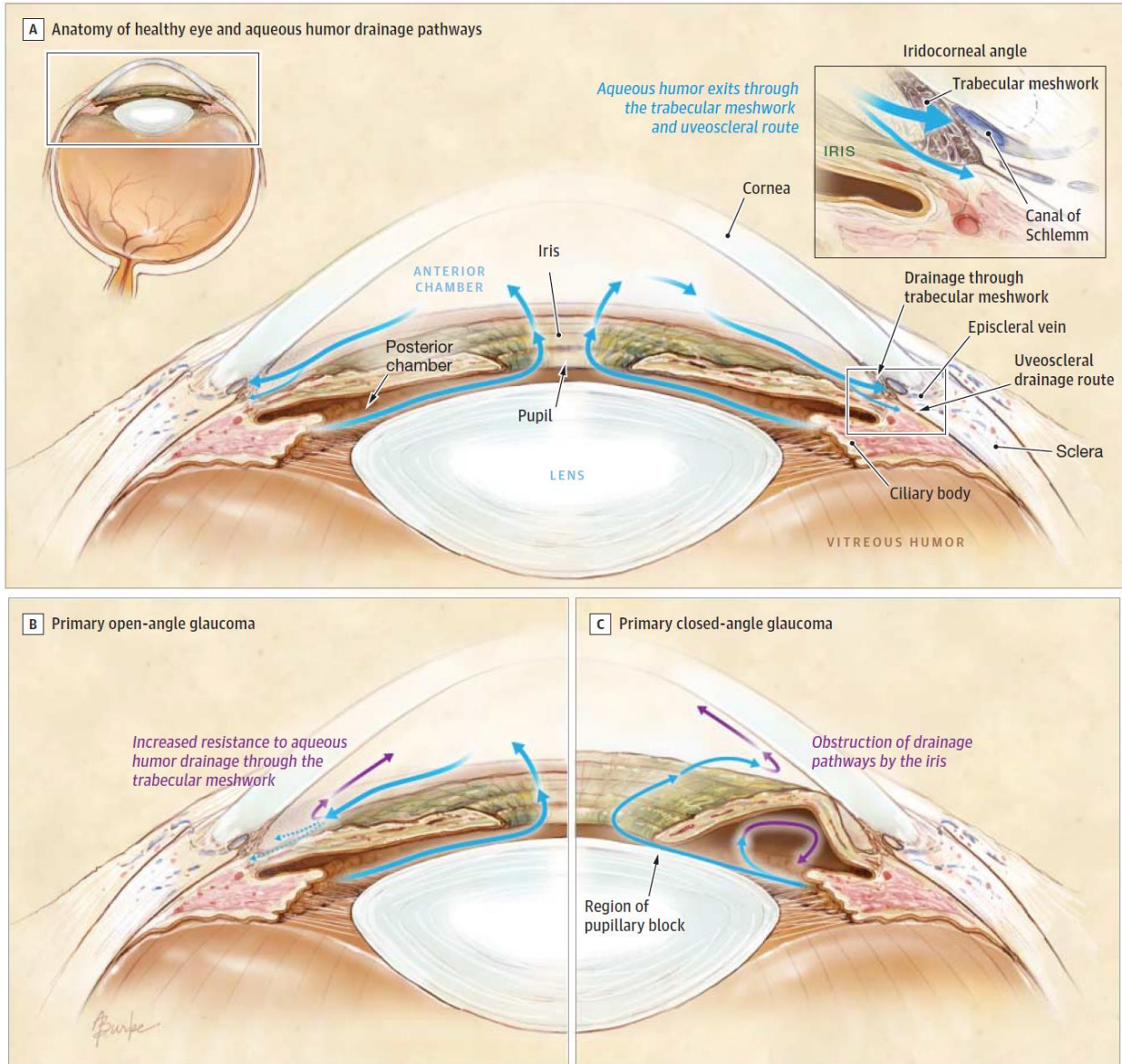


Fig 1.1 Aqueous humor drainage pathways of healthy eyes

Intraocular pressure is defined by balance between secretion of aqueous humor by the ciliary body and its drainage through two independent pathways: the trabecular meshwork and uveoscleral outflow pathway. In open-angle glaucoma, there is increased resistance to the

outflow of aqueous humor through the trabecular meshwork unlike angle-closure glaucoma where the drainage pathway is obstructed by the iris. A transverse section of the discussed anatomy is shown in figure 1.1 (7). The site of aqueous outflow in the eye is obstructed by the iris, resulting in a 'closed' eye. The obstruction is the main feature differentiating primary open-angle glaucoma from closed-angle glaucoma. Increased intraocular pressure can lead to mechanical stress and strain on the lamina cribrosa, causing its compression, deformation, and remodeling. These changes can result in the disruption of axonal transport, which may lead to the accumulation of vesicles and disorganization of microtubules and neurofilaments in the prelaminar and post-laminar regions of the optic nerve. Along with these structural changes, there may also be mitochondrial dysfunction in retinal ganglion cells and astrocytes, leading to a compromised energy supply during periods of metabolic stress caused by elevated intraocular pressure. These changes are associated with glaucoma and can result in vision loss if left untreated (7).

It is true that reduction in elevated IOP helps in slowing down the progression of degenerative changes in glaucoma and was believed to be the sole reason for the death of RGCs. However, studies have shown that only one-third to half of the patients with glaucoma have elevated IOP at the initial stages (8-10). Despite the strong relation between glaucoma and elevated IOP, a substantial number of people with elevated IOP never develop glaucoma (11). Like many degenerative diseases, glaucoma progresses without any symptoms until the disease has caused critical amounts of neural damage. The resulting vision loss quickly degrades the quality of life and the ability to perform daily activities. Therefore, early intervention and adherence is essential to slow the progression of the disease.

1.2 Glaucoma diagnosis, treatment, and management

Angle-closure glaucoma and open-angle glaucoma vary vastly in the symptoms and diagnostic evaluation. Angle-closure can show symptoms of pain radiating from the eye, visual impairment, conjunctival hyperemia, sometimes nausea and vomiting with a tense, rock-hard globe. In contrast, open-angle glaucoma does not show symptoms until it has reached an advanced stage. Most visual defects do not lie in the same part of the field of two eyes and are therefore compensated by binocular vision (12). Therefore, most people with open-angle glaucoma generally report no symptoms. A survey by Gramer et al. reported that nearly 10-20% of patients were already unable to drive a vehicle at the time of presentation at the clinic (13).

Appearance of the optic nerve head (ONH) and retinal nerve fiber layer changes with the death of retinal ganglion cells and nerve fiber loss (11). These changes can be identified during ophthalmoscopic examination of the ONH. Therefore, the importance of early and appropriate ophthalmoscopic examination cannot be overstated. Unfortunately, there is no single perfect reference for the diagnosis of glaucoma and early diagnosis can be difficult. Given the uncertainty surrounding glaucoma, primary care physicians have an important role in the diagnosis of the disease by referring patients with a family history of glaucoma to undergo a complete ophthalmologic examination.

1.2.1 Treatment

The primary goal of glaucoma treatment is to slow the progression of this disease and preserve the patient's quality of life. The decrease in quality of life may occur before diagnosis, emphasizing the importance of early diagnosis and treatment. Currently, the only form of treatment that has shown promise and proved to be efficacious for the prevention of glaucoma is reduction of intraocular pressure (IOP). Reduction of IOP in patients with open-angle glaucoma

can be achieved through regular application of eyedrops, laser therapy, and/or surgery (14, 15). In Ocular Hypertension Treatment Study, a study conducted by Kass MA et al., patients with ocular hypertension (high intraocular pressure but no signs of glaucomatous damage to the optic nerve or visual field) were randomized to treatment vs. no treatment. At the end of a 5 year follow up, 4.4% of the medicated group vs. 9.5% of the untreated group developed signs of glaucoma (15). Furthermore, a study conducted by The Early Manifest Glaucoma Trial performed a similar test where patients were divided into treat vs. no treatment with the only difference being that all patients had a clear diagnosis of glaucoma. At the end of a six-year study it was determined that progression of glaucoma was lower in the treat group (45%) than in the untreated group (62%) (16).

Substances of various classes are available for topical use to reduce intraocular pressure. They differ in mechanisms of action, in the degree to which they lower IOP, their dosing, side effects and cost (17). Extensive network meta-analysis on topical medication showed that prostaglandin analogs (bimatoprost by 5.61 mm Hg, latanoprost 4.85 mm Hg, travoprost 4.83 mm Hg, tafluprost 4.37 mm Hg) lowered IOP to the greatest extent, followed by beta blockers, alpha2-adrenergic agonists, and carbonic anhydrase inhibitors (17). In poorly adherent patients or severe cases laser or incisional surgery may be offered as the first step (7).

Patient adherence to glaucoma medication is essential to mitigating risks of irreversible blindness and propagation of disease leading to invasive surgery. Factors such as old-age, misinformation or lack of information, differing priorities and emotional factors pose risks to patient adherence to topical medication (18, 19). Artificial intelligence can play a major role in improving adherence by mitigating some of these risks.

1.3 Role of Artificial Intelligence

Recent technological advances in the healthcare industry have helped health care providers with better diagnosis and management of medical diseases. Specifically, access to patient data and images has drastically increased putting the spotlight on deep learning, a subset of traditional machine learning algorithms, to develop a completely autonomous system to diagnose ophthalmic conditions through ocular imaging (20). In the case of diabetic retinopathy, such a system already exists (21).

Unfortunately, unlike diabetic retinopathy, a standard reference for diagnosing glaucoma does not exist but the implementation of AI in ophthalmology and the use of it can mitigate the subjectiveness associated with diagnosing it. Given the ongoing integration of technology in medicine, it is speculated that artificial intelligence is likely to play a major role in ophthalmology.

Artificial intelligence (AI) methods have shown potential in aiding the discovery of novel biomarkers for glaucoma, a condition that can cause irreversible vision loss (22). By extracting meaningful features from complex data modalities, AI can assist in the early detection of glaucoma and the development of new drugs and treatments. A collaborative effort between AI systems and clinicians can lead to advancements in both glaucoma research and clinical practices, paving the way for improved patient outcomes.

1.4 Objectives and an overview

The primary objective of this dissertation is to leverage data to develop novel methods to guide interventions in glaucoma care and management. Glaucoma care and management is multi-fold and with this dissertation we aim to use technology and data to target issues regarding patient adherence to glaucoma medication. Broadly, Chapter 2 focuses on developing a human

activity recognition (HAR) model trained on data collected from patient handling of eye-drop bottles while using a nose pivoted drop delivery device (NPDD) called GentleDrop™ (23). Chapter 3 presents the effects of sensor data coordinate transformation on human activity recognition models, for the purposes of housing the sensor package in alternative locations and configurations on the eye drop bottle. Chapter 4 addresses the need for a versatile HAR model i.e., developing a model that is trained with added correlated features and in the absence of a NPDD. Figure 1.2 below shows how the dissertation is organized.

Patients with glaucoma often require lifelong treatment and follow-up care to preserve vision. Blindness caused by glaucoma is preventable; however numerous studies have shown that access to eye care resources and adherence to treatment are still major obstacles (24, 25). Chapter 2-4 delves into the opportunities presented by glaucoma-specific data to bring artificial intelligence into clinical practice. Specifically, the chapters highlight barriers associated with glaucoma medication adherence and pursuing data-driven approaches to improve them. Self-administering eye-drops poses a unique set of challenges especially in the aging population. It requires dexterity, coordination and follow-up, skills which put a lot of responsibility on the patient (18). Chapters 2-5 present a possibility of using data collected through smart eye-drop bottles, specifically acceleration, gyroscopic events, handling force with and without the use of a delivery aid to develop a human activity recognition model to provide an insight into a patient's adherence behavior. Allowing care providers to intervene at the right time and improve a patient's adherence to glaucoma medication.

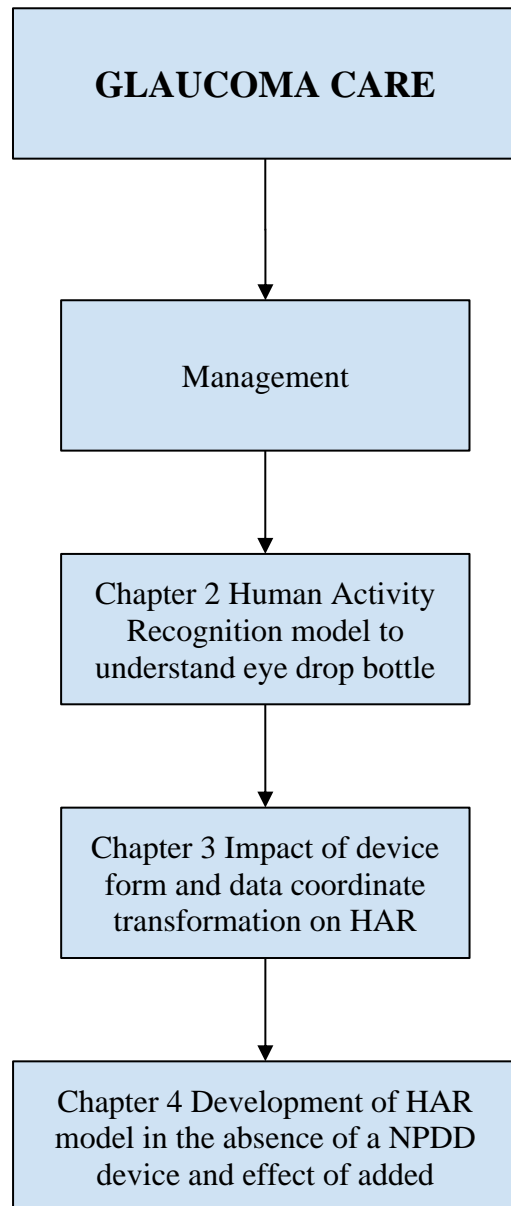


Fig 1.2 Overview of the chapters in this dissertation

CHAPTER 2

Effective management of glaucoma relies on timely diagnosis and consistent medication by patients. Many patients however, face difficulty in adhering to their medication routine, particularly with eye drops. This can lead to poor treatment outcomes and potential loss of vision. Several strategies have been developed to tackle the issue of poor adherence, including the use of smart eye drop bottles to track and monitor usage. The following chapter aims to develop and evaluate a human activity recognition model trained on data gathered from a smart eye drop bottle to improve patient adherence to glaucoma medication. By identifying and addressing adherence barriers, we can enhance patient outcomes and promote the effective management of this disease.

2.1 Introduction

Glaucoma is one of the leading causes of blindness worldwide and affects over 70 million individuals globally and more than 3 million Americans every year (1). It is a complex disease that is often asymptomatic in its early stages and can lead to irreversible vision loss if not appropriately managed. Worldwide, the number of people with primary open angle glaucoma is projected to exceed 111.8 million by 2040 (26). With so many people predicted to be affected by this disease, it has become increasingly important to leverage available data to develop tools that can assist care providers and patients in effectively managing it.

Currently, there is no cure for glaucoma, and treatment focuses on reducing intraocular pressure (IOP) to slow down the progression of the disease (15, 16). The most used, and the most effective, treatment approach is the use of topical eye drops, which must be self-administered by the patient multiple times a day (14, 15). However, patient adherence to the medication regimen is a significant challenge in glaucoma management, with adherence rates as low as 50%

measured through health insurance claims data (27), pharmacy data (28) or electronic monitoring (29). Nonadherence to glaucoma medication can be attributed to various factors such as complex dosing regimens, forgetfulness, lack of knowledge about the disease, high costs and passive learning style (30, 31). The administration of eye drops for glaucoma medication also presents unique challenges that can affect adherence, particularly in the elderly population, where the prevalence of glaucoma is increasing (30, 32). Self-administering eye drops requires adequate vision and hand-eye coordination, which is a demanding task for the elderly and patients with later stages of glaucoma (18). This issue needs to be addressed to ensure that glaucoma patients adhere to their medication and prevent further complications of the disease.

Currently there are a few options in the market that help improve patient adherence to glaucoma medication. Travatan dosing aid is one such device developed by Alcon that assists patients in taking travoprost and records when drops are administered (33, 34). 93% of doses were recorded accurately when patients took the device home. The dosing aid recorded extra drops when it was carried in a briefcase or backpack because it records the depression of the lever and not the administration of the drop itself. The Lumigan Compliance Aid is a device that aims to improve patient adherence to their medication regimen by providing audible and visual reminders at the designated dosing time (35). This device features a timed flashing light and an optional sound alarm that alerts the patient to take their medication. After 24 hours, if the bottle is not removed from the cradle, the device resets itself for the next reminder. However, this device has its limitations, as it only supports medications that are dosed once daily and does not help with instillation or squeezing of the bottle. Kali Care and Aptar Pharma collaborated to develop a device that improves patient adherence to glaucoma medication using a monitoring system that incorporates smart sensors, data analytics, and cloud services (36). The monitoring

system is called the Kali Drop, a small and wireless device that detects the opening and closing of medication bottles and tracks the number of drops administered. The software can also recognize individual patient's application patterns and detect if someone else uses the device. However, a study of 28 patients reported that five devices had device-related errors that resulted in incorrect data recording.

Current devices in the market, albeit helpful, put the responsibility back on the patients to address issues of non-compliance. With all the data available through current technology, it has become imperative to analyze them and develop a better solution that is more active in its intervention to improve adherence with glaucoma medication. Studies have shown that increase in awareness about the disease, demystifying complex regimen and customizing treatment plans to suit patient specific needs might improve adherence with glaucoma medication (37, 38).

The identification of individual activities involved in administering eye drops is necessary to improve post-diagnosis management. In cases where a patient administers multiple drops due to improperly dispensed previous drops, identifying the sequence of individual activities helps track when a drop was correctly administered. This method avoids recording every action as "dispensed," which could bias the data to project positive adherence. Additionally, the GentleDrop™ device was designed to aid in administering a drop while ensuring that it is applied at the right angle and position. This feature eliminates the need to administer multiple drops. The human activity recognition model can also mitigate the risk of false results due to surveys reporting patients faking their eye drop usage. In such cases, patients have been known to empty a bottle just before reporting their usage to a doctor. Recording data in such cases biases the results and highlights the importance of integrating a human activity

recognition model with GentleDrop™. Doing so can exponentially improve monitoring of patient adherence to glaucoma medication.

The following sections of this chapter focus on developing a data-driven model to potentially improve glaucoma management. Described later is the design and development of a Human Activity Recognition model that is trained on data collected from patient handling of the eye-drop bottle. With the introduction of adherence aid devices such as the Lumigan Compliance Aid and Kali Drop, the demand for a low-cost and compact device that can recognize human activity from available data, has risen. Deep learning models are capable of learning features from raw datasets, making feature engineering obsolete and not requiring domain expertise.

2.2 Method

The GentleDrop™ paired with a commercial inertial measurement device using a 3D printed holder collects data on acceleration and gyroscope events in the x, y and z directions. The adhered inertial measurement unit (IMU) is the primary source of data around which a human activity recognition (HAR) model is built. The HAR model is trained to identify different actions associated with eye drop bottle handling. The following sections cover the data collection and details of the HAR model.

2.2.1 Prototype Hardware

The device consists of three major components: the inertial measurement device, the 3D printed holder and the GentleDrop™. The inertial measurement device/accelerometer is a TI multi-standard sensor tag with an on-board accelerometer and gyroscope with a BLE receiver and microcontroller linked to it. The sensortag assembly is considerably bulky and unwieldy which will affect the recorded data, removing it from a real-world scenario. Therefore, the

commercial inertial measurement device is tethered to the body of the '*GentleDrop*TM' using a 3D printed holder (figure 2.1), allowing for easier handling, and using the device as intended.

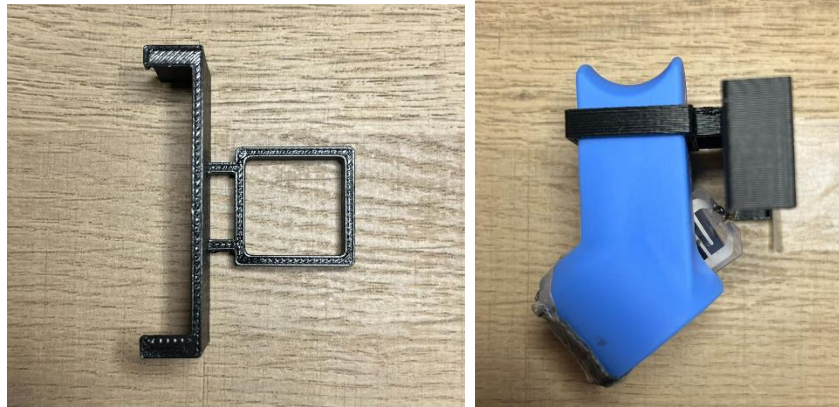


Fig 2.1 3D printed holder designed to house the IMU and prototype.

The *GentleDrop*TM is a trademark device developed by Retinal Care Inc. that acts as a sleeve into which a glaucoma medication bottle can be inserted. The purpose of this device is to facilitate ideal conditions for administering eye-drops. The *GentleDrop*TM has an ergonomically designed concave end that can be placed on the bridge of the nose of a patient. In addition to being a physical aid while administering glaucoma medication, the *GentleDrop*TM also helps in the development of the HAR model by stabilizing data during the administration. Pictures of the *GentleDrop*TM, the commercial inertial measurement device and the 3D printed holder can be seen in the figure 2.2. The measurement device is powered by a USB-B port connected to a power source while the data is recorded through a Bluetooth connection to a mobile application developed by Retinal Inc as well.

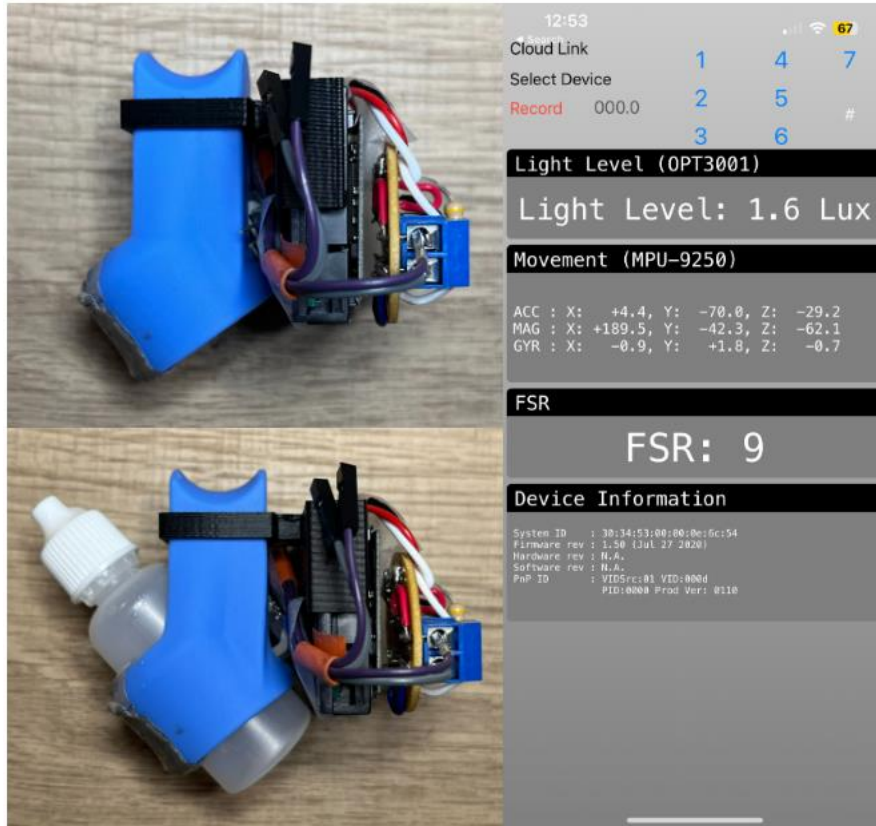


Fig 2.2 The entire assembly with the prototype, the IMU, 3D printed holder and GentleDrop™. A screengrab of the mobile application used to record and view inertial readings.

2.2.2 Data Collection

Data was collected from three bottles of the same type, shape, and size. Since no pressure sensors were being used, it was determined that the type of bottle was irrelevant to the development of the model. Though bottles of varying shapes and sizes could affect the movement of the prototype and consequently the acceleration data, the impact was determined to be minimal. The two most common ways of administering eye drops is with the patient laying down on their back or sitting upright and bringing the bottle to their eye level. The latter is most preferred by patients self-administering eye-drops and the GentleDrop™ is designed to aid them in this activity. Therefore, for this model data was collected for the latter case with the patient sitting upright. The following set of activities were identified as the most typical way of handling eye drop bottles with the GentleDrop™: picking up the bottle & the GentleDrop™, inserting the

bottle into the GentleDrop™, opening the cap, elevating the bottle to eye level and placing the GentleDrop™ on the bridge of the nose, squeezing the bottle to administer a drop, lowering the bottle, replacing its cap, separating the bottle and the GentleDrop™ and then placing bottle & GentleDrop™ at rest without any patient contact. Volunteers cycled through these activities for each eye-drop bottle until they were empty. Data collection started with the eye drop bottle & the GentleDrop™ being initially at rest without any contact with the volunteer. This was followed by the volunteer picking up the bottle and the GentleDrop™ to assemble. The volunteer then opened the bottle cap while sitting upright. Next, the volunteer elevated the bottle to eye-level and placed the GentleDrop™ on the bridge of their nose. For the next activity that involved dispensing a drop, care was taken not to administer the drop directly into the eye of the volunteer, but instead having it fall into a crucible that was simultaneously elevated to eye level. The bottle was then lowered, followed by replacing the cap. The GentleDrop™ and the bottle were then disassembled and the two were then left at rest, completing one cycle of activities. These sets of activities were cyclically repeated until the bottle was empty. The preliminary model was trained on the eight activities mentioned above. Following the performance of the first model one more model was trained with a combination of activities being paired as one. In model 2, the lower and close activity were labeled as a single activity. Data was collected real-time over Bluetooth at a frequency of 15 - 24 Hz. For every data point, the acceleration and gyroscope values in each of the cartesian coordinates were recorded.

A total of 1407 cycles were completed i.e., 1407 drops were administered by multiple volunteers for the dataset used in model 1 and 2. To determine sufficiency in data collected, the model was run over multiple cycles with data being added at a batch of 10,000. As seen in the

graph in figure 2.3, the overall model accuracy plateaued at 887,000 datapoints, which made up the train set while the test set was made up of 104,000 datapoints.

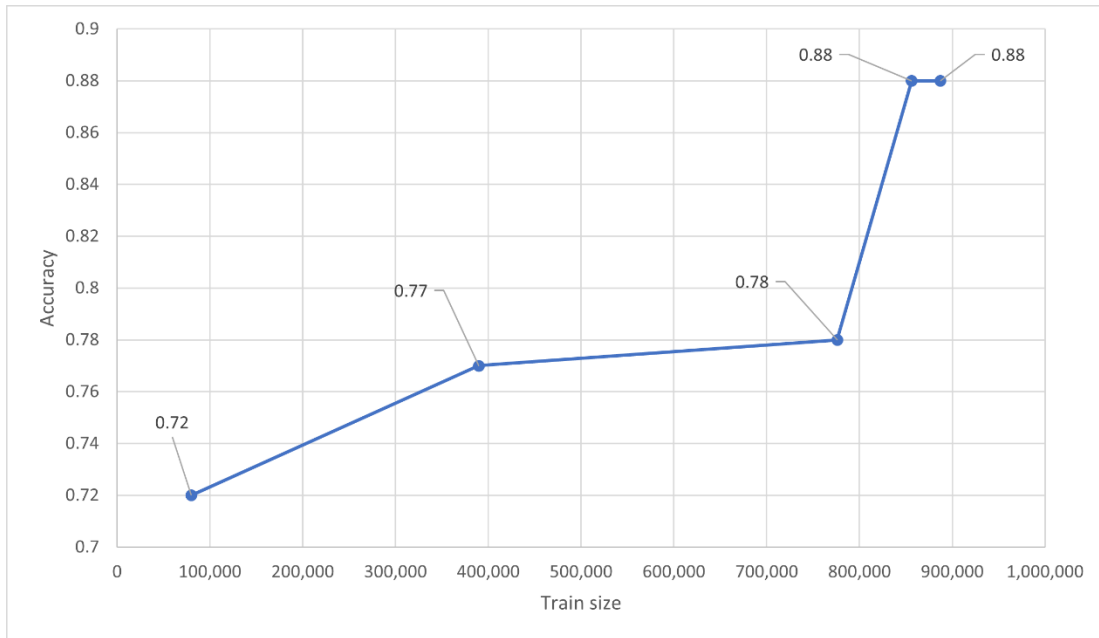


Fig 2.3 The change in model overall accuracy as the training dataset is increased.

Supervised learning algorithms, such as HAR models, necessitate labeled data to train the model. To generate labeled data, voice recording integrated with a python script was implemented to automate the labeling process using the end times of each activities and datapoints recorded. Volunteers were asked to announce the activity label, ‘A’ through ‘H’ as seen in figure 2.4, at the end of its corresponding activity. A python script was developed to extract the end time of each activity label from the voice recording and match it to the end time of a datapoint. All end times were matched and identified after which the activities were labeled in the sequence they were performed.

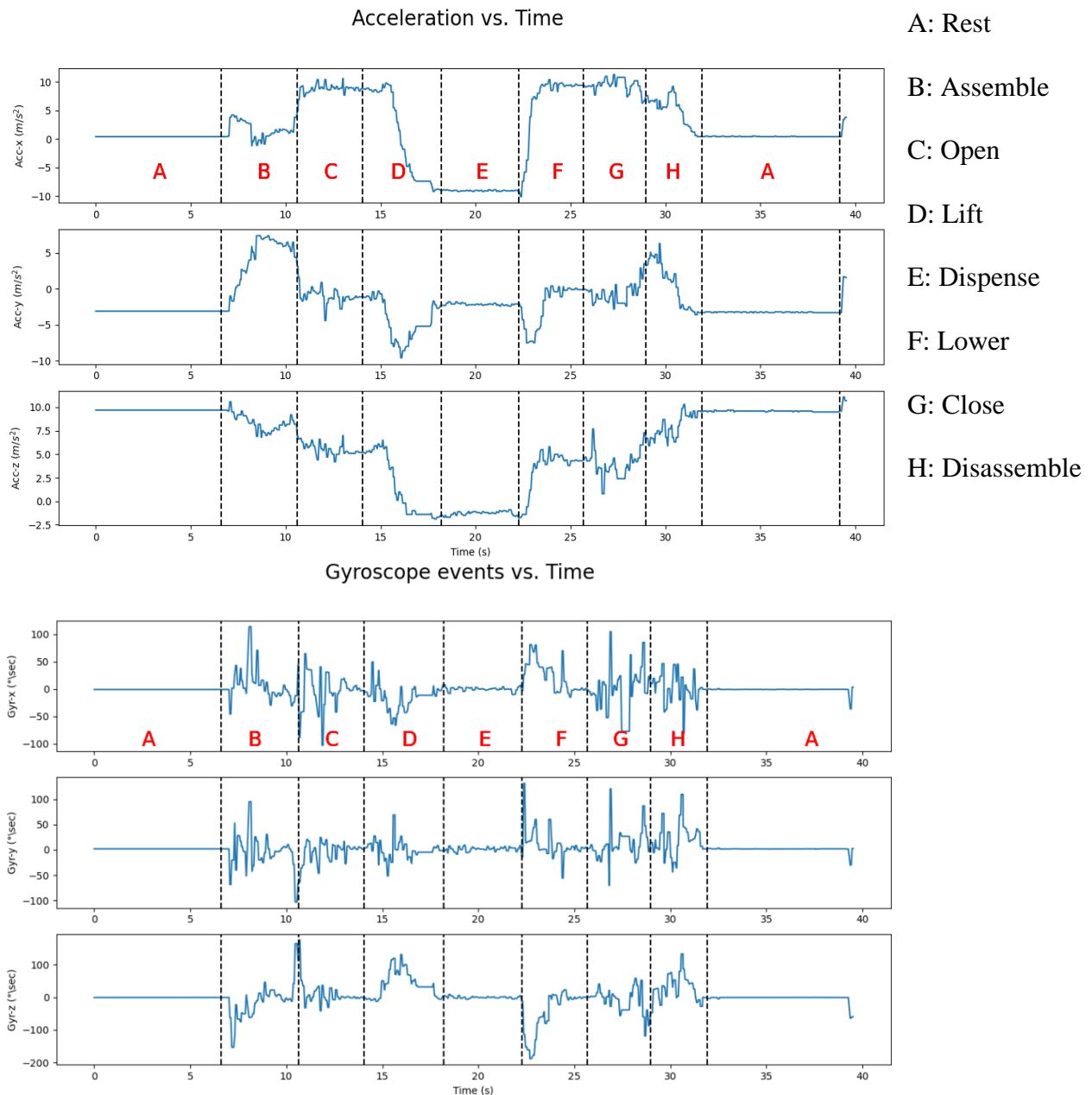


Fig 2.4 The change in acceleration and gyroscope values in each of the cartesian coordinates as the bottle is initially at rest (A), then the bottle is inserted into the GentleDrop™ (B), followed by opening the cap (C) and lifting the bottle (D) to the bridge of the nose and squeezing the bottle (E). The bottle is then lowered (F) and the cap is closed (G) before separating the bottle and GentleDrop™ (H).

2.3 Data preprocessing

Neural networks that are appropriate for time series classification rely on a supervised learning approach, which involves preparing the data in a specific manner to enable the model to associate signal data with a corresponding activity class. A common data preparation technique that is used for both classical machine learning methods and neural networks is to segment the input signal data into windows of signals, with each window containing a duration of one to a few seconds of observation data. This method is often referred to as a sliding window approach. The objective of human activity recognition is to deduce the actions of one or more individuals based on sensor data. To achieve this, a fixed length sliding window approach is often employed for feature extraction. When splitting a stream of sensor data into windows for human activity recognition, there is a possibility that some windows may not capture the transition between different activities. To mitigate this risk, overlapping windows were implemented, where each window contains observations from both the current and previous windows.

Each window was labeled based on the most frequent activity mode occurring in it. In the first two models, a window size of 40 data points was used with a 25% overlap, corresponding to a time interval of 1-2 seconds, as seen in figure 2.5. The data was divided into multiple 2D windows of size 40 x 6, with each window consisting of six features: acceleration and gyroscope events in the x, y, and z directions.

The window size and percentage of overlap are different for every model and selected based on the model's response to its variation.

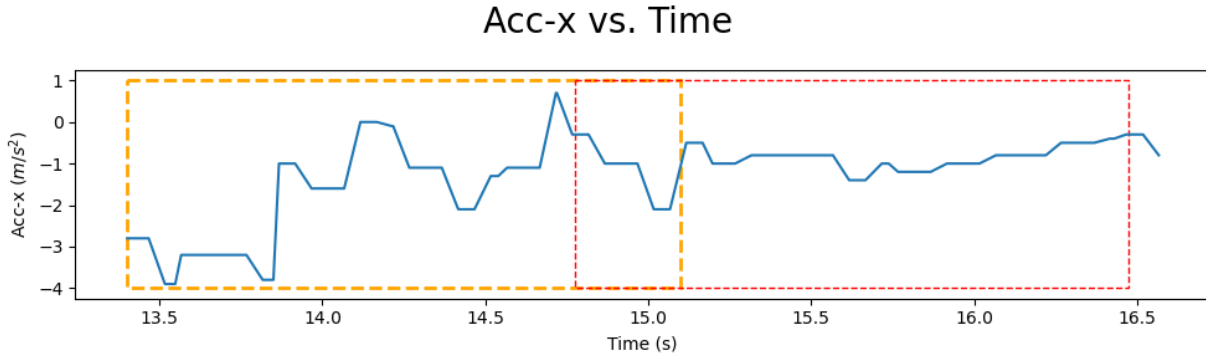


Fig 2.5 Data segmented into windows with an overlap to avoid transitional errors.

2.4 Model

To develop a human activity recognition model, a long short-term memory (LSTM) recurrent neural network (RNN) was trained on multiple eye-drop bottles of the same medication. With LSTM being a neural network method, it does not require domain expertise to manually engineer input features. The model can learn from raw time series data. LSTM network models can learn and remember long sequences of input data. They are intended for use with data that is comprised of long sequences of data, up to 200-to-400-time steps and is a good fit for this problem. The model can also support multiple parallel sequences of input data, such as each axis of the accelerometer and gyroscope data. The model learns to extract features from sequences of observations and how to map the internal features to different activity types.

As mentioned earlier, two different LSTM RNN models were evaluated: model number 1 for the 8 original activity labels, model number 2 for a combination of lower and close. Model two was developed as an optimization based on the performance of the first. Based on preliminary results it was determined that activities such as lifting and replacing the cap showed some similarity. Therefore, the model would perform better if these activities were labeled as a single activity, allowing it to differentiate between activities clearly.

Data from the three bottles was collected and labeled. Figure 2.6 below shows the distribution of each labeled activity in the dataset. As seen below, the “Dispense” activity has the lowest number of datapoints and the “Rest” activity has the highest number of datapoints. This is expected as the device remains at rest for an extended period while the activity of dispensing a drop occurs 2-3 times a day and takes only a few seconds. Data collected from bottles 1 and 2 were combined to be used as the training set while data from bottle 3 was used as the test set. The training set was then split using a stratified k-fold ($k = 10$) cross validation method allowing for an even distribution of all classes/activities within each split, while also avoiding overfitting.

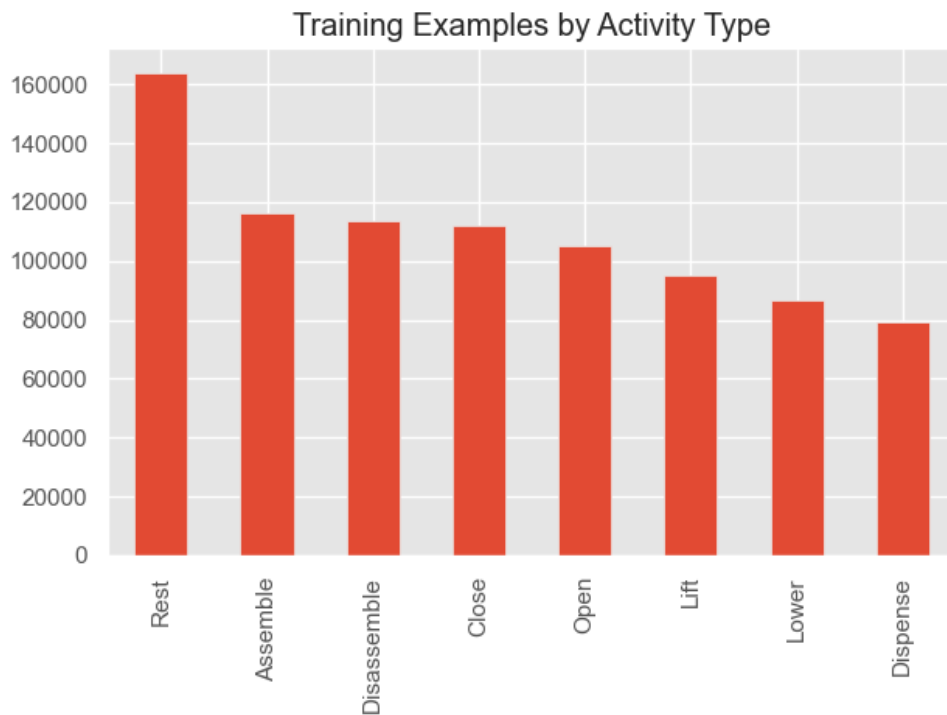
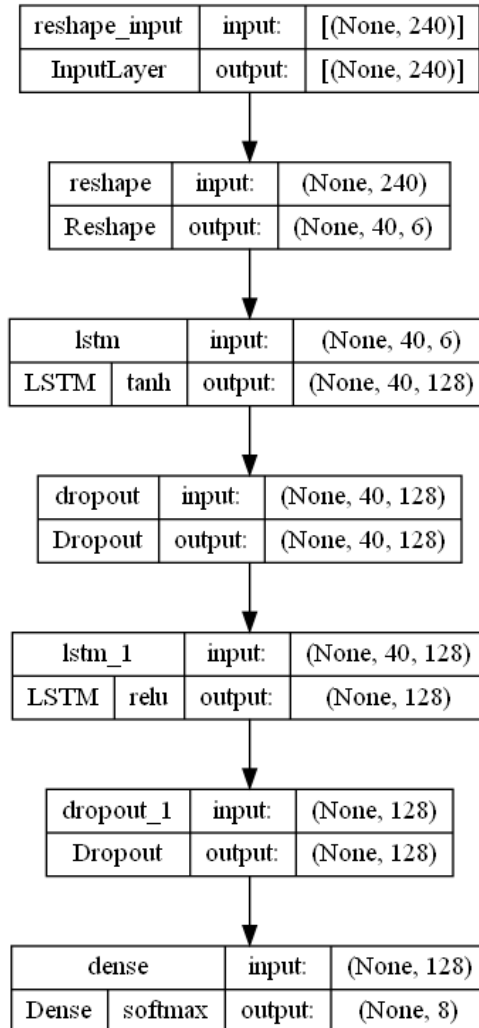


Fig 2.6 Distribution of each activity across the dataset

The data features were scaled to values between 0 and 1 to enable faster optimization in supervised learning algorithms such as neural networks. To feed the data to the neural network, a sliding window technique was applied. The long short-term memory recurrent neural network (RNN) used in this study was built and trained using the Python library Keras (39). Figures 2.7

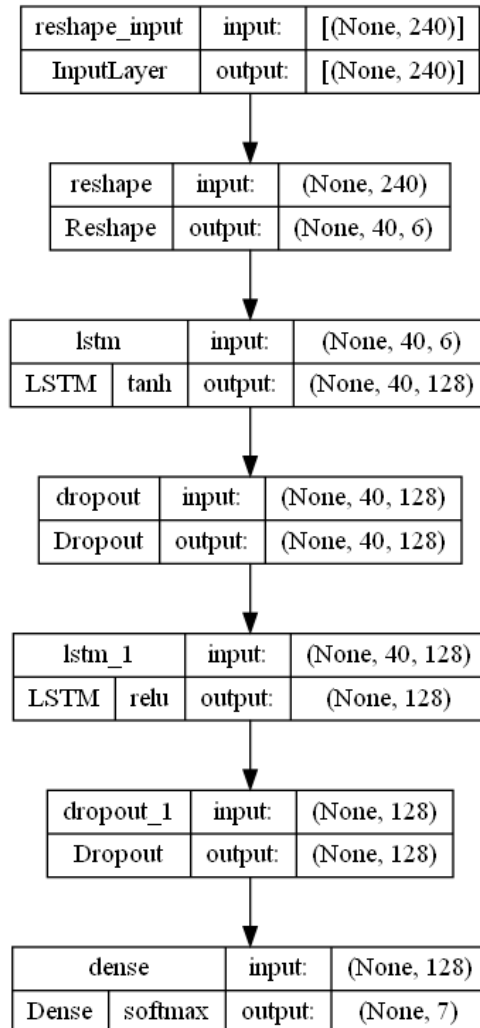
and 2.8 summarize the architecture of the neural network across the two models. The model consisted of two LSTM layers, each with 128 filters and a rectified Linear Unit (ReLU) activation function on the second layer. This allowed the model to learn complex features. To prevent overfitting, a dropout layer was included after each LSTM layer. The dropout layer randomly assigned zero weights to 50% of the input units, simplifying the network. The final layer was a fully connected layer with 7 units and a soft-max activation function. The value in each unit represents the conditional probability for a particular activity given the original features. During training, the Adam optimizer was used to minimize the loss function, with default values for β_1 , β_2 , and ϵ set to 0.9, 0.999, and $1e-7$, respectively, as these values have been found to be generally effective for most neural network architectures.



A sequential model, a linear stack of layers is used.

1. Reshaping the input to 40 x 6, with 40 data points and 6 features
2. LSTM layer with 128 units and return sequences to ensure the next LSTM layer receives sequences and not scattered data.
3. A dropout layer after every LSTM layer to avoid overfitting.
4. Finally, a fully connected layer with a SoftMax activation returns an array of size 8. One unit representing each activity.

Fig 2.7 The long short-term memory recurrent neural network architecture used for the first model.



A sequential model, a linear stack of layers is used.

1. Reshaping the input to 40 x 6, with 40 data points and 6 features
2. LSTM layer with 128 units and return sequences to ensure the next LSTM layer receives sequences and not scattered data.
3. A dropout layer after every LSTM layer to avoid overfitting.
4. Finally, a fully connected layer with a SoftMax activation returns an array of size 7. One unit representing each activity.

Fig 2.8 The long short-term memory recurrent neural network architecture used for the second model with combined classes.

2.5 Results

The two models were evaluated by calculating the overall accuracy across a stratified k fold model. Additionally, performance metrics such as recall, precision, and specificity were computed for each activity along with a combined confusion matrix. Recall evaluates the model's ability to correctly identify the activity, while precision measures the proportion of correctly predicted activities. Specificity for an activity represents the model's ability to correctly classify all other data points as negative, not belonging to the desired activity. Model no. 1 trained on a dataset with 8 original labels (Rest, Assemble, Open-cap, Lift, Dispense, Lower, Close-cap, Disassemble) yielded an overall test accuracy of 86%. The performance metrics and confusion metric for this model is shown below.

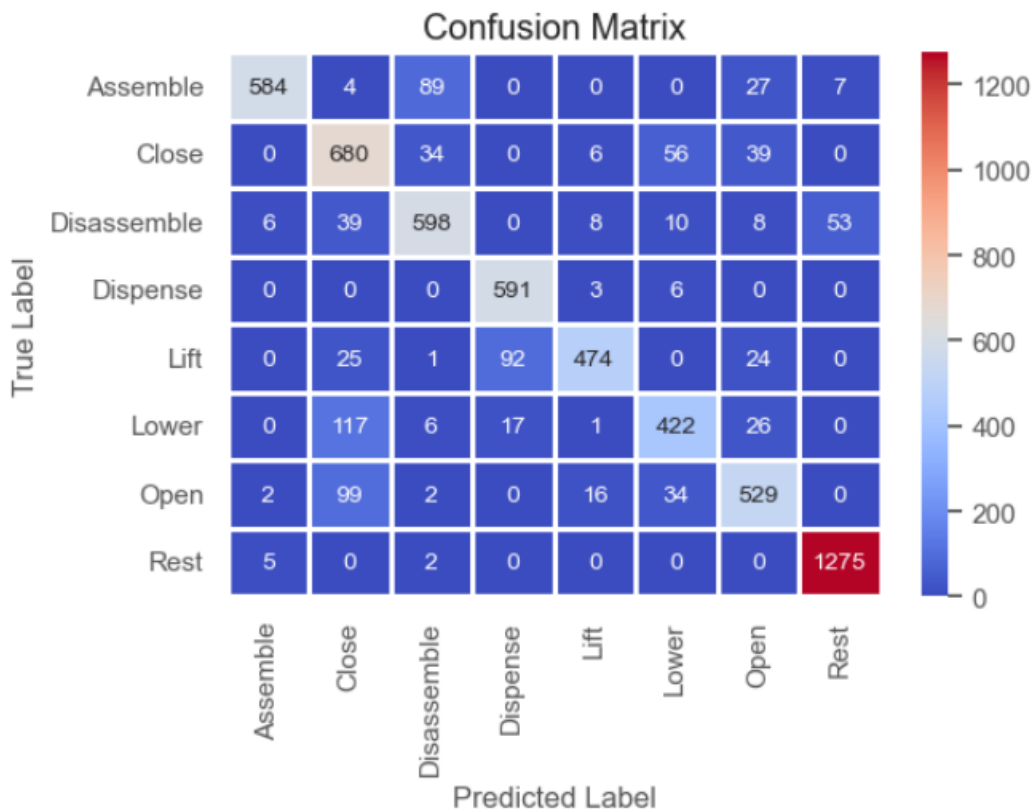


Fig 2.9 The confusion matrix from the model trained on all eight activities with the use of GentleDrop™

Table 2.1 Activity - specific performance metrics for the model trained on all eight activities with the use of GentleDrop™.

| Activity | Recall/Sensitivity | Specificity | Precision |
|------------------------------|---------------------------|--------------------|------------------|
| Assemble | 0.82 | 0.99 | 0.98 |
| Close/Close cap | 0.83 | 0.94 | 0.71 |
| Disassemble | 0.83 | 0.97 | 0.82 |
| Dispense | 0.98 | 0.98 | 0.84 |
| Lift | 0.77 | 0.99 | 0.93 |
| Lower | 0.72 | 0.98 | 0.80 |
| Open/Open cap | 0.78 | 0.97 | 0.81 |
| Rest | 0.99 | 0.98 | 0.96 |
| Overall accuracy: 86% | | | |

The model trained on the new label ‘LC’, which is a combination of the ‘lower’ and ‘close’ labels, yielded an accuracy of 88%. The confusion matrix and performance metrics computed from it are shown below.

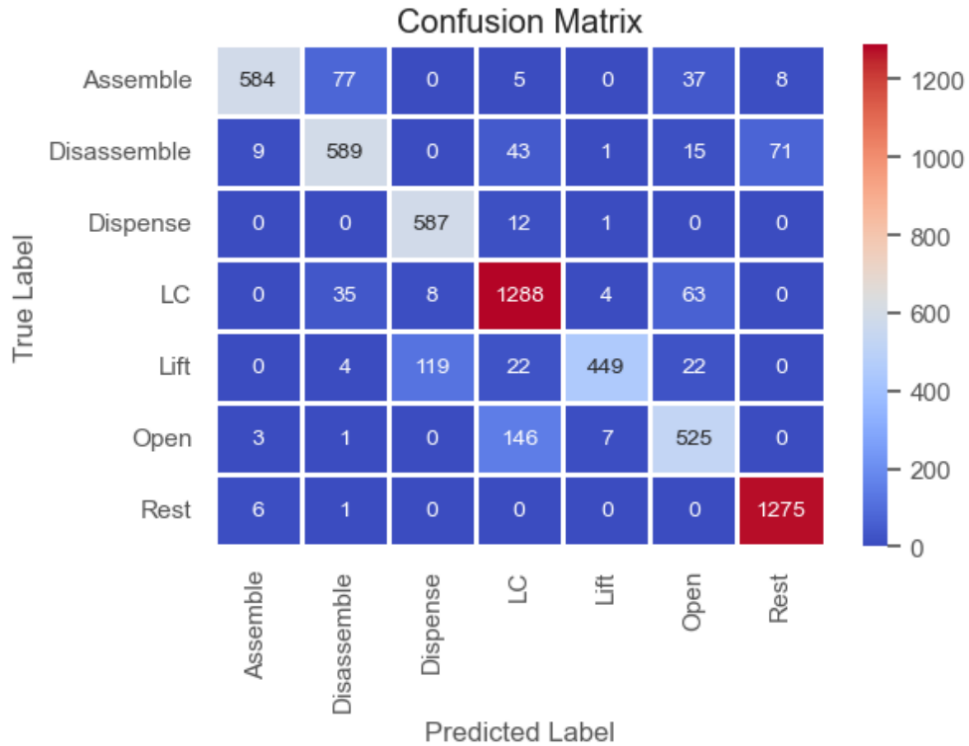


Fig 2.10 The confusion matrix from the model trained on 7 activities and the combined label LC with the use of GentleDrop™.

Table 2.2 Activity - specific performance metrics for the model trained on seven activities and the combined label ‘LC’ with the use of GentleDrop™.

| Activity | Recall/Sensitivity | Specificity | Precision |
|------------------------------|--------------------|-------------|-----------|
| Assemble | 0.82 | 0.99 | 0.97 |
| Disassemble | 0.81 | 0.97 | 0.83 |
| Dispense | 0.98 | 0.97 | 0.82 |
| LC | 0.92 | 0.95 | 0.85 |
| Lift | 0.73 | 0.99 | 0.97 |
| Open | 0.77 | 0.97 | 0.79 |
| Rest | 0.99 | 0.98 | 0.94 |
| Overall accuracy: 88% | | | |

2.6 Discussion

This chapter focuses on developing a deep learning model that can leverage the data collected from smart eye-drop bottles to mitigate some of the challenges associated with patient adherence to glaucoma medication. A HAR model was developed using a long short-term memory recurrent neural network and trained on eye-drop bottle handling data that was collected from a prototype device consisting of an inertial measurement unit, a Bluetooth communication device and the GentleDrop™. To increase patient adherence, it was determined that successfully predicting the action of dispensing a drop into the eye of a patient was important. Therefore, the model must be independent of the type of bottle used and actions were predicted using the accelerometer and gyroscope data only. It was assumed that the use of GentleDrop™ created clear patterns within the data and made it easier to predict the ‘Dispense’ action without the need of an FSR. Two models were developed, each consisting of the same data but with a different combination of labels. Model 1, containing 8 labels that show the 8 steps involved in administering a drop successfully, achieved an overall accuracy of 86%. Model 2 trained on 7 labels where the lower & close activity classes were combined and achieved an overall accuracy of 88%. The stratified k-fold cross validation method was used to ensure an even spread of labels across the training and validation sets as well as to avoid overfitting.

The model with the least number of labels performed the best. This is expected because the model finds it easier to differentiate between the action of dispensing a drop and any other action. As mentioned earlier, the use of GentleDrop™ was predicted to make it easier to differentiate the action of dispensing a drop by stabilizing the action of doing so. Generally, a patient would hold the eye-drop bottle over their eye and aim the drop at the center of the eye. This action is unstable when compared to doing the same with a GentleDrop™. In comparison,

model 1 was poor in predicting the dispense activity as seen from the confusion matrix in figure 2.9 and the corresponding performance metrics. The time taken to dispense a drop was short, ranging from 1 sec to 2 seconds, resulting in lower number of datapoints under the activity 'Dispense' and is a possible reason for a relatively poor predictive performance. Based on previous results, model 2 was trained on data with lower-close labels combined. The model was able to achieve an overall accuracy of 88%. The 'Dispense' and 'LC' activities are misclassified as 'Lift' and 'Open' which explains the low recall percentages. The action of lifting the eye-drop bottle and dispensing a drop are separated by a short activity of placing the GentleDrop™ on the nose. This activity only lasts from 0.5 to 1 second, thus blending the activity of lifting and dispensing a drop leading to misclassification. Similarly, 'Open' and 'Close' activities show little variation when reading accelerometer data. Therefore, many data points belonging to class 'LC' are misclassified as 'Open'. Overall, the performance of the two models can be improved with the use of a more well-developed prototype. The current form of prototype is unwieldy which affects the handling of the assembly. A miniaturized version of the Bluetooth sensor and accelerometer would possibly yield values of acceleration and gyroscope that are more representative of a real-world scenario. Additionally, the model has been trained and tested on data where the activities are cycled through fast and consecutively. In a real-world application, with possibly 2-3 drops daily, the eye-drop bottle would remain at rest for an extended period. Therefore, the model must be tested on data that mimics this scenario to get a true measure of its performance.

Although there are limitations, the integration of HAR models and smart bottles can provide care providers with crucial data about patients' behavior regarding their glaucoma treatment plan. This data can be used to educate patients on the best practices for self-

administering eye drops and to actively monitor patient-specific bottle usage. Analyzing this data can help identify non-adherent patients, and care providers can intervene as needed to improve patient outcomes.

CHAPTER 3

Human activity recognition faces some challenges with performance when dealing with inertial data recorded at varying orientations (40-42). Without transformation, in theory, classifying data can be costly, time-intensive and produce inadequate results where the model is unable to identify the right actions (43). Moreover, the model is trained on a single orientation and introduction to similar data with a different orientation will affect model performance. In this section, we specifically focus on developing transformations of inertial data that can be used in the previously discussed HAR model. Data collected from an inertial sensor (accelerometer and gyroscope) consists of three-dimension position values. We convert the raw accelerometer data collected from the inertial sensor into a uniform reference coordinate system using rotation matrices and Euler angles. Finally, a model trained on this transformed data is discussed.

3.1 Development of transformation for alternate sensor hardware orientation

Data recorded from the device (GentleDrop™-IMU) can originate from varying orientations and placements. The idea behind using signal transformation is to generate uniform signals from different angles (43). The basic idea is to transform all input signals into the same global reference coordinate system, thus making it easier to train a model.

A reference frame comprises an origin that represents a point in space with three-unit vectors or axes that are made up of a right-handed system. There are numerous reference frames that can be used to represent a system based on its application, such as sensor frame, body frame or earth-centered, earth fixed frame (ECEF) also known as geocentric reference frame. As mentioned in the previous section, transformation of data reference frames is required to help standardize datasets and develop better HAR models.

Rotations have been applied to the same dataset used in chapter 1. It consists of acceleration and gyroscopic values of the sensor package in the three coordinate axes (x,y,z). The sensor package, which is attached to the GentleDrop™ which in turn houses the eye drop bottle, is considered as a single system all represented by the sensor frame. For ease of use and future application, the sensor reference frame is transformed to a North-East-Down reference frame (NED) that is defined by ECEF coordinates.

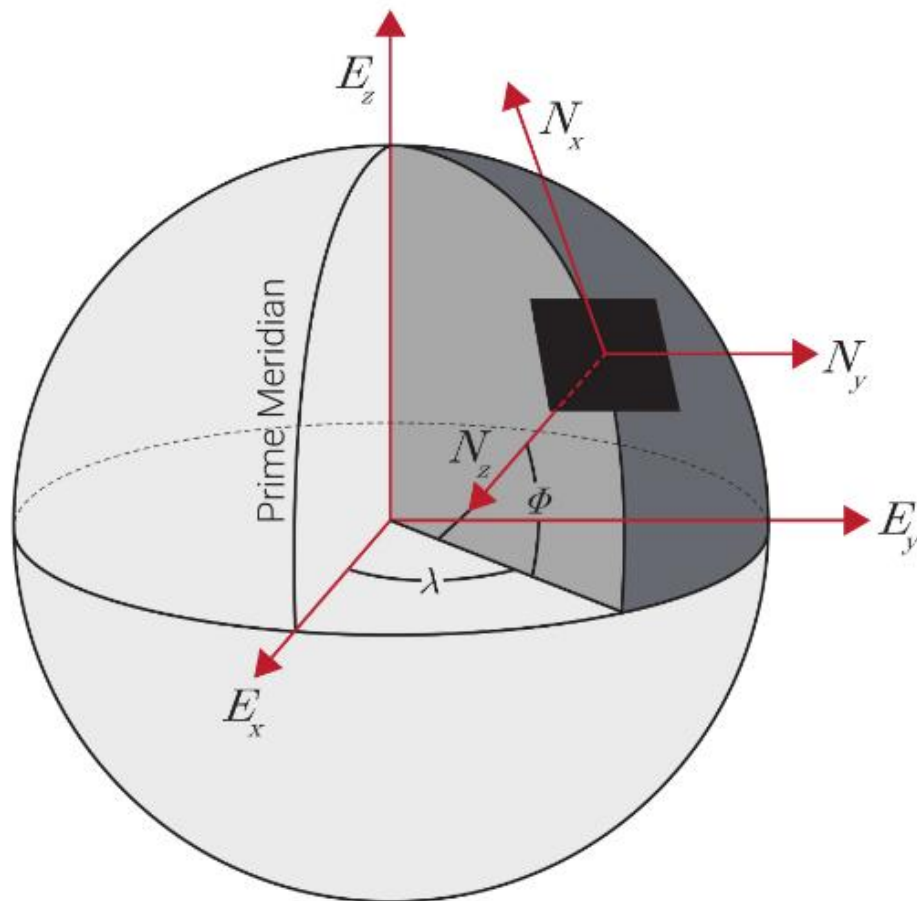


Fig 3.1 ECEF and NED Frames with a description of each axis and its direction.

The ECEF reference frame is a global reference frame commonly used in navigation and object positioning. The cartesian coordinate system in the ECEF reference frame uses the E_x , E_y and E_z axes orthogonal to each other with the origin at the center of the earth. As shown in figure 3.1, the E_z axis points through the North Pole, E_x through the intersection of the IERS Reference

Meridian (IRM) and E_y completes the right-handed system. The NED frame is a reference frame defined by the ECEF coordinates. Often this frame is fixed to the body of the device to which the sensor is attached. In our case, where the sensor and the setup are comparatively the same size, the sensor reference frame is considered as the body reference frame. In the NED frame, the North and East axes form a tangent with the earth's surface at its present position, assuming a WGS84 ellipsoid model of the earth (44). As seen in figure 3.1, the NED frame contains three axes in which N_x points to true north, the N_z axis points to the interior of the earth and N_y points East. By providing a common reference framework, it enables data from different sources to be combined and analyzed more easily.

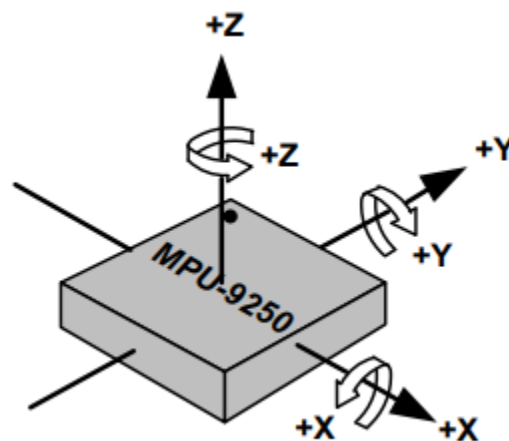


Fig 3.2 Orientation of Axes of Sensitivity and Polarity of Rotation for Accelerometer and Gyroscope.

Conversion of inertial data in sensor reference frame to NED reference frame can be done through two methods using rotation matrices, or quaternions. A rotation matrix uses a 3×3 matrix to convert a vector from one reference frame to another. The rotation matrix is made through the combination of rotation matrices of each axis of rotation. To determine the rotation matrix for each axis of rotation the initial frame of reference of the sensor/ body frame is required. This gives us the relative orientation of the sensor with respect to the global frame of reference

(NED). The initial frame of reference of the sensor used here is shown in figure 3.2 (45). The X-axis points to the east, Y-axis to the north and Z-axis pointing up in the local frame. With this information the yaw (Ψ), pitch (θ) a roll (ϕ) angle to transform local frame to NED frame of reference is known.

The transformation matrix $R_b^n(\Theta) \in \mathbb{R}^{3 \times 3}$ transforms sensor data in X, Y and Z defined in body frame, v_o^b , into data in the NED frame of reference, \dot{p}^n , based on the rotational differences between the two frames of reference represented by Euler angle notation Θ [1]. $R_b^n(\Theta)$ is defined by the standard convention zyx [3] and consists of three rotations, one for each Euler angle [2] (46). The elements defined in body frame, v_o^b , is rotated by ϕ , then by θ and finally by Ψ . The order of rotations is not commutative due to the compounding effect of the rotational order.

$$\dot{p}^n = R_b^n(\Theta)v_o^b \quad [1]$$

$$R_{x,\phi} = \begin{bmatrix} 1 & 0 & 0 \\ 0 & \cos \phi & -\sin \phi \\ 0 & \sin \phi & \cos \phi \end{bmatrix}, R_{y,\theta} = \begin{bmatrix} \cos \theta & 0 & \sin \theta \\ 0 & 1 & 0 \\ -\sin \theta & 0 & \cos \theta \end{bmatrix}, R_{z,\psi} = \begin{bmatrix} \cos \psi & -\sin \psi & 0 \\ \sin \psi & \cos \psi & 0 \\ 0 & 0 & 1 \end{bmatrix} \quad [2]$$

$$R_b^n(\Theta) = R_{z,\psi}R_{y,\theta}R_{x,\phi} \quad [3]$$

$$R_b^n(\Theta) = \begin{bmatrix} \cos \psi \cos \theta - \sin \psi \cos \phi + \cos \psi \sin \theta \sin \phi & \sin \psi \sin \phi + \cos \psi \sin \theta \cos \phi \\ \sin \psi \cos \theta & \cos \psi \cos \theta + \sin \phi \sin \theta \sin \psi & -\cos \psi \sin \phi + \sin \theta \sin \psi \cos \phi \\ -\sin \theta & \cos \theta \sin \phi & \cos \theta \cos \phi \end{bmatrix} \quad [4]$$

3.1.1 An example of transformation of collected inertial data.

Inertial data collected from eye-drop bottle is converted from the sensor frame to North-East-Down reference frame. The dataset is saved as a .CSV file and can be read in as a pandas or dask data frame. Pandas data frame is well known and commonly used when working with ML models. Though pandas data frames are usually very efficient, it does struggle to work with very large datasets. Of course, the lack of performance can also be attributed to the performance of the *'processing computer'*; use of the right library is an easier fix. The current dataset contains over 1 million data points and processing it using the pandas data frame consumes more memory and energy. Dask Data Frame (47) is a collection that parallelizes workloads involving Data Frames making it easier to process large datasets. It achieves this by breaking up the Data Frame into many smaller Pandas Data Frames that are partitioned along the index. To execute a Data Frame operation, Dask creates a task graph and performs operations on the constituent Data Frames in a way that minimizes memory usage and increases parallelism by sharing and deleting intermediate results. Dask maintains the Pandas API, which simplifies scaling up Data Frame workloads for users who are familiar with Pandas (47). To enable conversion, the accelerometer and gyroscope data is extracted from the database and stored in NumPy arrays. NumPy arrays provide a fast and efficient way to perform mathematical operations on large arrays of data (48). In the case of sensor data, the arrays are quite large. NumPy arrays allow us to perform mathematical operations, such as addition, subtraction, and multiplication, on entire arrays of data at once, rather than having to loop through each element in the array individually. This can significantly improve the speed and efficiency of our code, especially when working with large datasets.

Accelerometer and gyroscope data from Dask Data Frame is extracted as NumPy arrays, with each array consisting of signal data in each coordinate axis. Arrays are then converted to the NED frame of reference through rotation matrices obtained through relative orientation of the body frame. Figure 3.3 shows the accelerometer and gyroscope data after transformation.

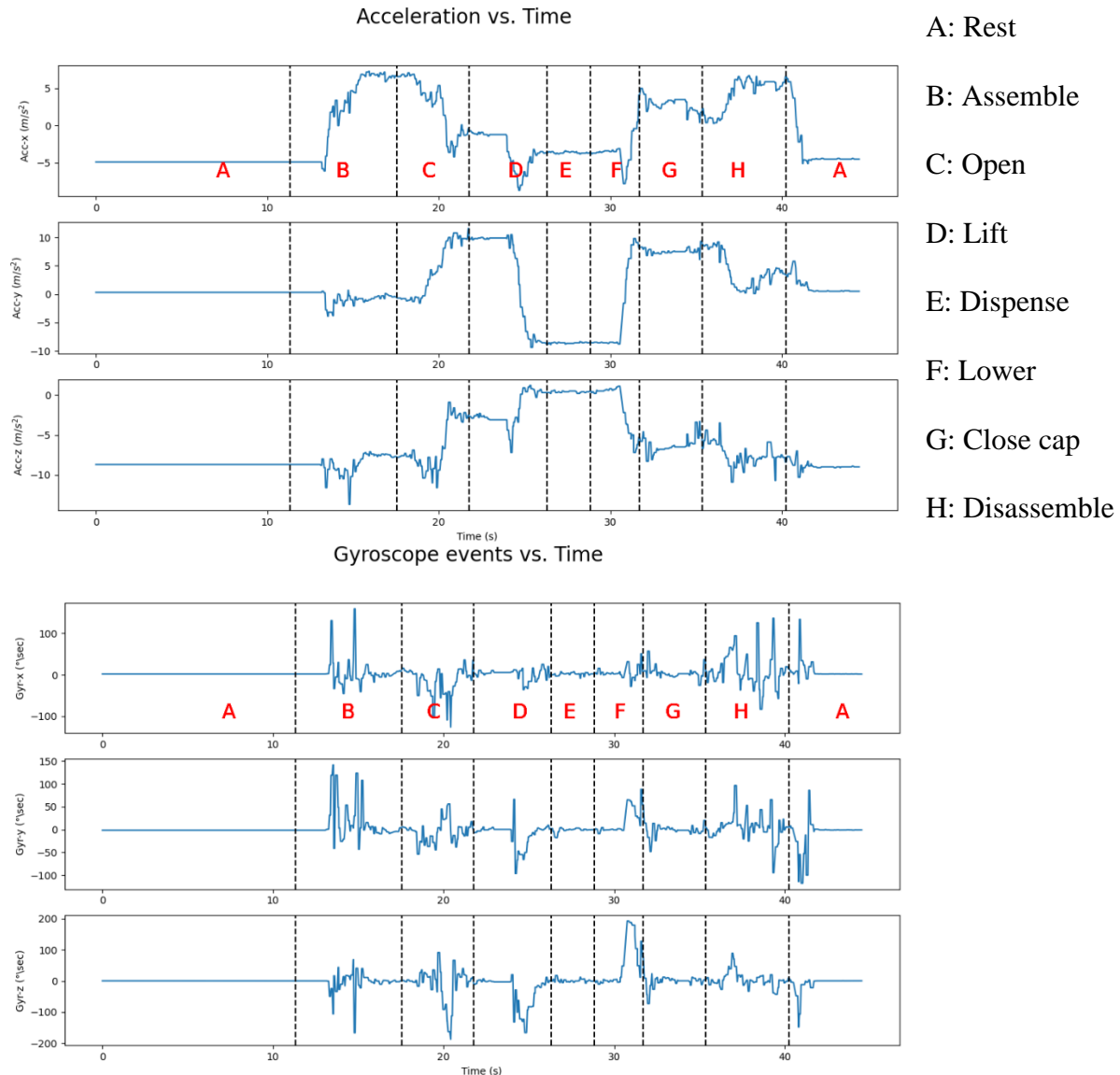


Fig 3.3 The change in acceleration and gyroscope values in each of the cartesian coordinates as the bottle is initially at rest (A), then the bottle is inserted into the GentleDrop™ (B), followed by opening the cap (C) and lifting the bottle (D) to the bridge of the nose and squeezing the bottle (E). The bottle is then lowered (F) and the cap is closed (G) before separating the bottle and GentleDrop™ (H).

3.2 HAR model developed on transformed accelerometer data as an added feature.

The advantage of transforming data is that it allows models to classify and recognize activities independent of the orientation of sensors. We considered seven user activities: rest, assemble, Open, Lift, Dispense, Lower-Close and Disassemble, with the same apparatus used in previous chapters. Each datapoint consists of acceleration and gyroscope events in the three coordinate systems. The HAR model was trained using the long short-term memory recurrent neural network built using the keras library in python (39).

The model is trained on data collected with the use of a NPDD (23), with the patient sitting upright and performing the previously mentioned steps/activities. The setup for model 1 is the same as the one used in chapter 2 (figure 2.1) where the inertial measurement device is tethered to the GentleDrop™ using a 3D printed holder. The device measures the acceleration and gyroscope events in the x, y and z directions. This data serves as the primary source to build a human activity recognition model and identify activities associated with handling an eye-drop bottle. The following chapter describes the details involved and the outcome of this experiment.

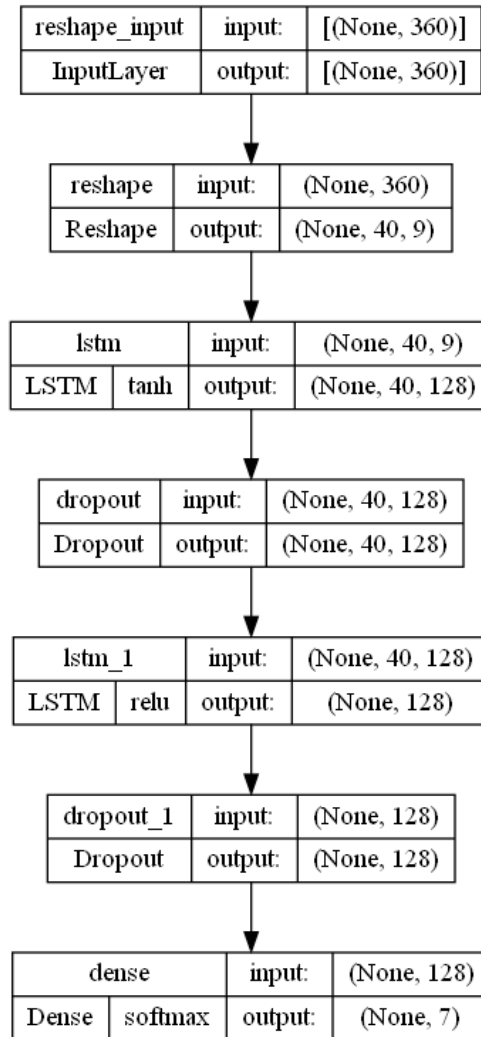
Data was collected from three eye-drop bottles of the same type, shape, and size, and volunteers performed a set of activities until the bottle was empty. The activities included picking up the bottle and the GentleDrop™, inserting the bottle into the GentleDrop™, opening the bottle cap, elevating the bottle to eye-level, and placing the GentleDrop™ on the bridge of the nose, squeezing the bottle, lowering the bottle, replacing its cap, separating the bottle and the GentleDrop™, and then placing the bottle and the GentleDrop™ at rest without any patient contact.

A human activity recognition model was developed using a long short-term memory (LSTM) recurrent neural network (RNN). The model was developed based on the performance

of the first model, as preliminary results suggested that lowering the bottle and closing of the cap were highly similar. This is understood as the activity of lowering the bottle is immediately followed by closing the cap with minimal change in orientation (of the bottle). Therefore, the model performed better when these activities were labeled as a single activity. The training set was created by combining data from bottles 1 and 2, and the test set was created using data from bottle 3. The training set was then split using a stratified k-fold cross-validation method, allowing for an even distribution of all classes/activities within each split while also avoiding overfitting.

The data features were scaled to values between 0 and 1 to enable faster optimization in supervised learning algorithms such as neural networks. A sliding window technique was applied to feed the data to the neural network, involving defining a fixed number of data points to be included in a single window and propagating it forward in the dataset with or without overlap. Each window was labeled based on the most frequent activity mode occurring in it. A window size of 40 data points was used with a 25% overlap, corresponding to a time interval of 1-2 seconds. The data was divided into multiple 2D windows of size 40 x 9, with each window consisting of nine features: acceleration, gyroscope events and transformed acceleration in the x, y, and z directions.

The LSTM RNN model is composed of two layers, with 128 filters in each layer, utilizing a rectified linear unit (ReLU) activation function. Following this, a dropout layer, and a final layer with 5 units and a soft-max activation function were included. To minimize the loss function during training, the Adam optimizer was utilized, with default values for β_1 , β_2 , and ϵ known to be effective for different neural network architectures. The Keras Python library was employed to construct and train the neural network, and the architecture is outlined in Figure 3.4.



A sequential model, a linear stack of layers is used.

1. Reshaping the input to 40 x 9, with 40 data points and 9 features
2. LSTM layer with 128 units and return sequences to ensure the next LSTM layer receives sequences and not scattered data.
3. A dropout layer after every LSTM layer to avoid overfitting.
4. Finally, a fully connected layer with a SoftMax activation returns an array of size 7. One unit representing each activity.

Fig 3.4 The long short-term memory recurrent neural network architecture used for the model trained on transformed sensor data as a feature.

The confusion matrices and performance metrics of the two models are presented below.

Performance metrics such as recall, specificity and precision are used to evaluate the models.

The model achieved an overall accuracy of 88%.

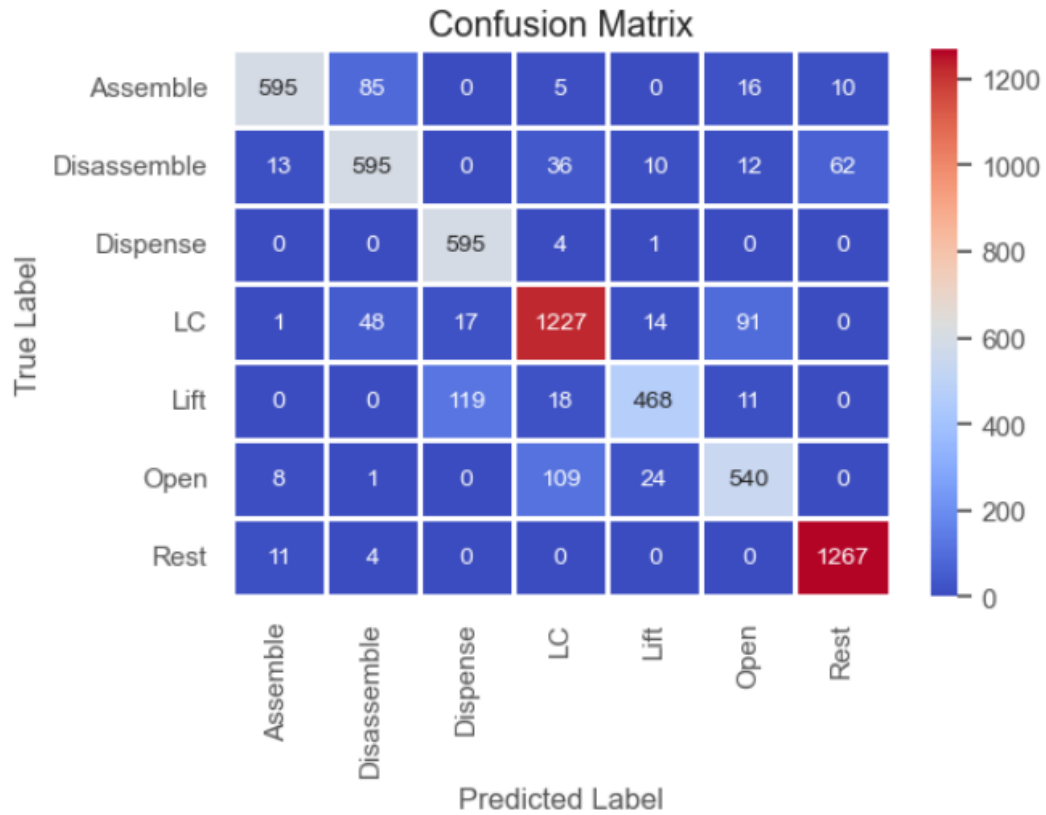


Fig 3.5 The combined confusion matrix of the model trained on transformed sensor data was added as a feature.

Table 3.1 Activity - specific performance metrics for the model trained transformed sensor data added as a feature.

| Activity | Recall/Sensitivity | Specificity | Precision |
|------------------------------|---------------------------|--------------------|------------------|
| Assemble | 0.84 | 0.97 | 0.95 |
| Disassemble | 0.82 | 0.95 | 0.81 |
| Dispense | 0.99 | 0.98 | 0.81 |
| LC | 0.88 | 0.98 | 0.88 |
| Lift | 0.76 | 0.98 | 0.91 |
| Open | 0.79 | 0.93 | 0.81 |
| Rest | 0.99 | 0.99 | 0.95 |
| Overall accuracy: 88% | | | |

3.2.1 Discussion

In this section we specifically focused on developing a human activity recognition model trained on inertial data transformed from local/body frame to a standardized frame such as North-East-Down reference frame.

The orientation of the sensor affects the activity recognition performance where a model trained on data received from one orientation would not be applicable to others. Therefore, building a model that is independent of device orientation is imperative to glaucoma care. An LSTM model was developed and trained on local frame sensor data and transformed sensor data added as a feature. The model achieved an overall accuracy of 88%.

When compared to preceding models, the performance of this model is promising yet requiring further optimization. As seen in the confusion matrix, the model confuses a few activities with others. For example, a high number of ‘Dispense’ activity data points were misclassified with ‘Lift’ activity data points. Same can be said about ‘Open’ & ‘LC’ activities. The activity of ‘Lifting’ the bottle and then ‘Dispensing’ a drop are very close to each other. The two activities are separated by the activity of placing the GentleDrop™ on the bridge of the nose.

The activity of placing the GentleDrop™ on the bridge and dispensing a drop are short and include stabilization enabled by the NPDD. Increasing the sampling rate data recording and using a sensor of higher sensitivity could result in a better model.

The methods used in this chapter are introductory and applicable to simple systems. The use of methods such as multimodal sensor fusion (49) and projection-based technique for device orientation transformation (41) have shown better results even at low sampling rates.

Despite its limitations, the HAR model trained on transformed data has shown promise and is one step closer to improving the lives of patients with glaucoma. The more we promote the model's versatility the higher the chances of analyzing patient behavior and accurately identifying non-adherent patients.

CHAPTER 4

In chapter 2 we presented the development of a human activity recognition system trained on patient handling of an eye-drop drop bottle with the use of GentleDrop™, a compliance aid. The model recognized human activity using inertial data in x, y and z directions with each datapoint being labeled with a certain activity. The activity of dispensing a drop successfully was stabilized by the GentleDrop™, aiding the model in predicting it. In this chapter, we aim to tackle the issue of increasing adherence in patients that do not practice the use of the GentleDrop™. Relying on inertial data would be difficult since it would experience destabilization during the administration of a drop. Therefore, added correlating features are required to address this issue.

The data is extracted from Dr. Omkar's doctoral study and published dissertation "Numerical Modeling to Understand the Pathophysiology of Glaucoma and Investigating Data-Driven Approaches for its Effective Management" (50).

4.1 Method

An inertial device is adhered to the eye drop bottle to record their movements & orientation and is integrated with a force sensitive resistor (FSR) to record the force exerted on the bottle while handling it. As mentioned, the adhered accelerometer is considered as the primary source of data while the recorded force bolsters the model when added as a correlating feature. With this data a human activity recognition model is trained to identify the different activities associated with handling an eye-drop bottle. The following chapter describes the hardware involved, data collection protocol, model used and outcome of this experiment.

4.1.2 Prototype hardware

The inertial measurement device is adhered to the glaucoma medication bottle to record data on its orientation. A prototype device is paired to the accelerometer to indirectly record FSR readings. The FSR is wrapped around the bottle like a label whose readings are recorded on a mobile device application developed by Retinal care Inc. The readings are conveyed via Bluetooth connection.

FSRs detect pressure through a change in resistance as a response to force applied. The FSR used here was custom built by Omkar & his team using a pressure-sensitive conductive sheet (velostat) and a conductive fabric (Faraday). To achieve the behavior of an FSR, a layer of velostat was sandwiched between two layers of Faraday as shown in figure 4.1A (50). Velostat is a non-conductive material made from polymeric foil integrated with carbon black. The sandwiched assembly of velostat and faraday was wrapped around eye-bottles and connected to the prototype to record data (figure 4.1B (50)). Each activity performed while administering the drop gave a unique FSR signature to it.

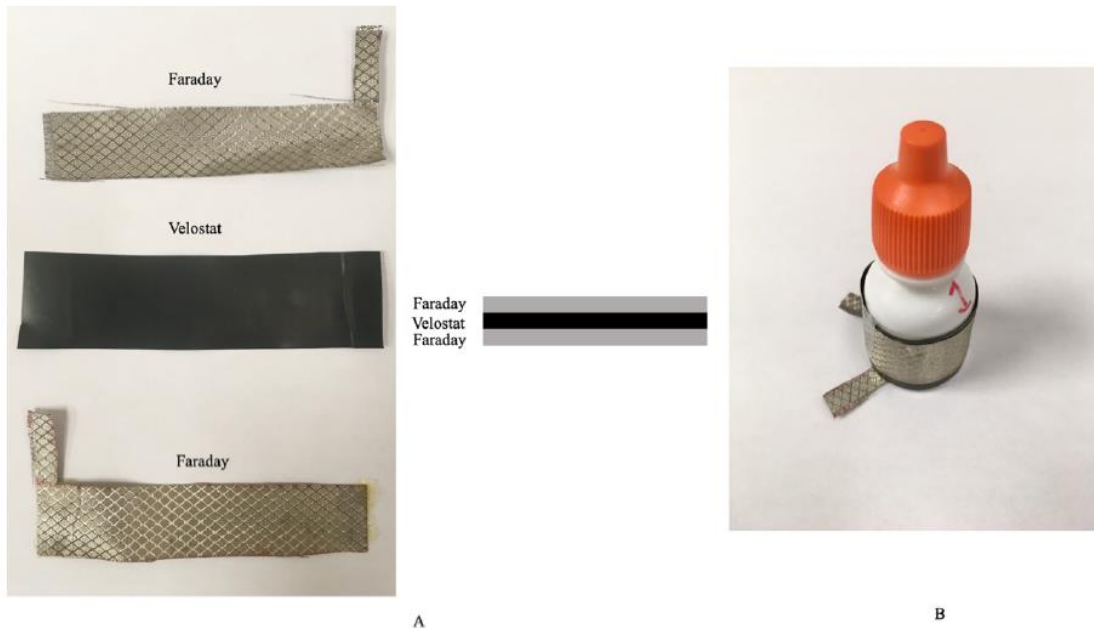


Fig 4.1 (A) The force sensitive resistor is made by sandwiching the velostat between two layers of faraday. (B) The FSR wrapped around the bottle.

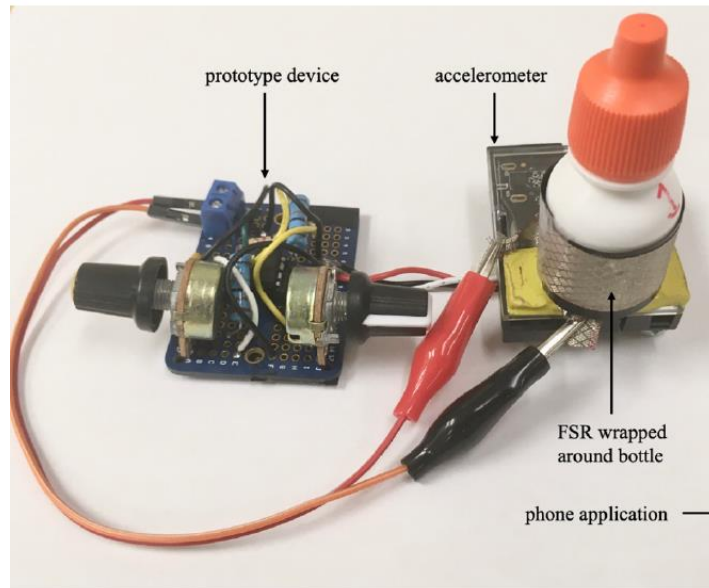


Fig 4.2 The prototype that integrates the FSR and accelerometer data assembled with the bottle.

4.1.3 Data collection

Data was collected from 5 different eye-drop bottles of different shapes and sizes and as a result a unique FSR was made for every bottle. Like the method used in chapter two, the operation of administering a drop of glaucoma medication was done with the patient sitting

upright, bringing the bottle up to their eye level. Of course, with no GentleDrop™, the eye-drop bottle was held right above the crucible and not resting on the bridge of the patient's nose. As done with previous experiments, care was taken to not dispense the liquid into the volunteer's eye. Instead, a crucible was placed over the eye to protect the volunteer while staying true to the action of dispensing a drop. The activities involved in successfully administering a drop were defined as follows: picking up the bottle and opening the cap, lifting the bottle to eye level, squeezing the bottle to dispense a drop, lowering the bottle, closing the cap, and placing the bottle at rest. These sets of activities were cyclically repeated until the bottle was empty. Each data point recorded the acceleration in x, y and z direction along with the FSR output as shown in figure 4.3. Opening and closing of the cap was labeled as a single activity.

To label data to build a HAR model using supervised learning, the mobile application was modified to record the start times of every activity. This data was fed into a MATLAB script to automate the process of labeling.

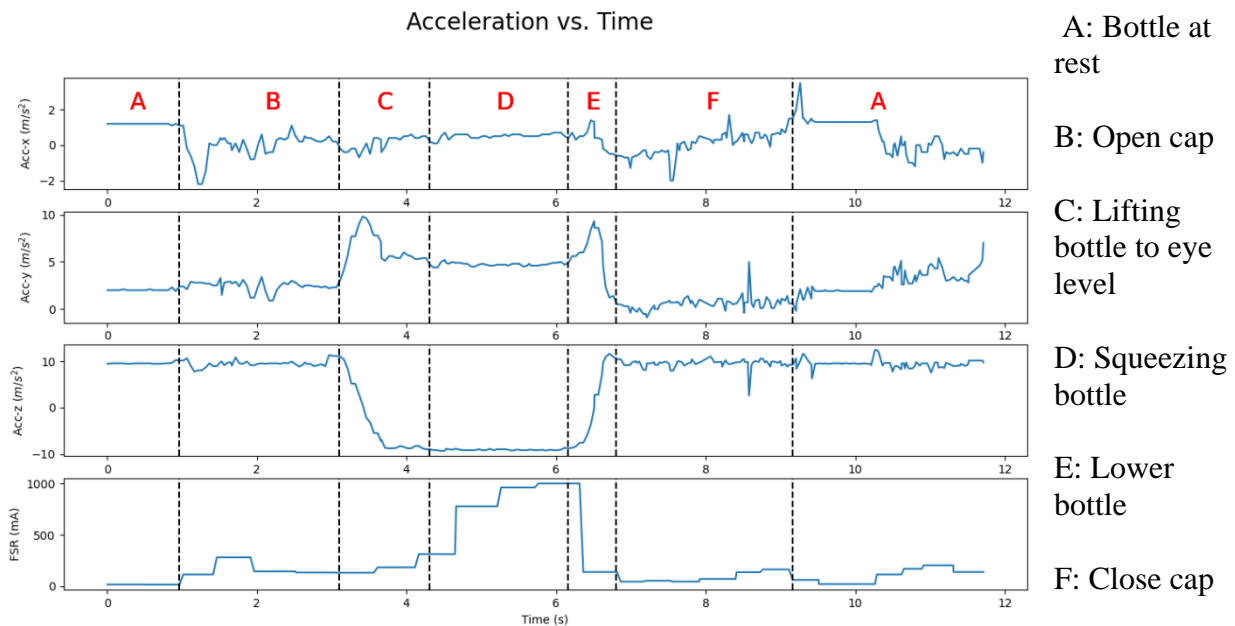


Fig 4.3 The behavior of FSR, and acceleration as each activity was performed over time.

4.2 Model

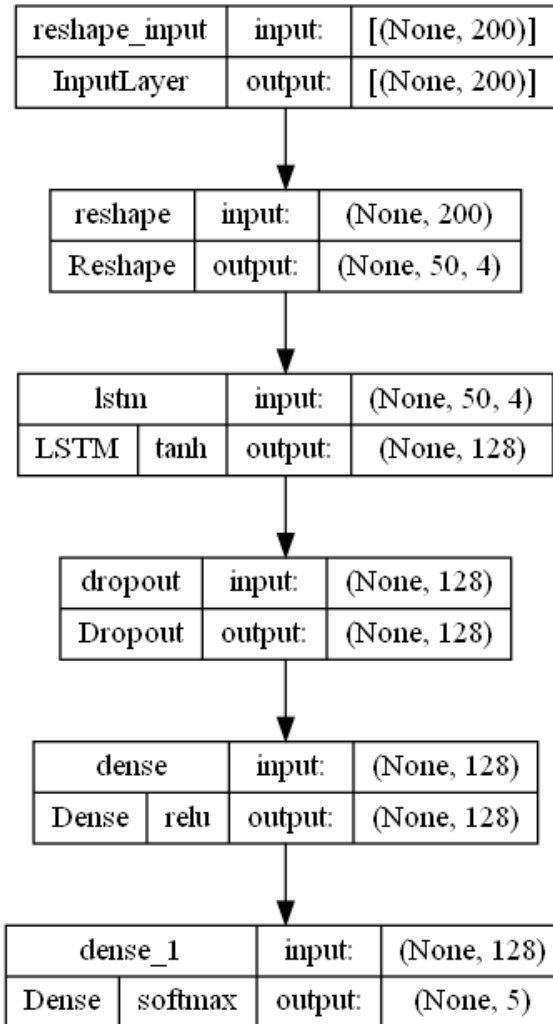
To develop a model for recognizing human activities, a recurrent neural network (RNN) with long short-term memory (LSTM) was used, which was trained on the data collected by Dr. Omkar. The LSTM RNN model was evaluated with the open-close activities labeled as a single activity.

To maintain a low cost, computationally, and improve the versatility of the model used in chapter 2, a similar setup and architecture has been developed for the current dataset. A distribution of data across the various classes/activities is seen in figure 4.4. Data from four bottles were combined and used as the training set, while data from the fifth bottle was used as the test set. The training set was stratified to have an even distribution of all activities/labels. A sliding window with 50 datapoints and a 50% overlap was used. The data was divided into multiple 2D windows of size 50 x 4, with each window consisting of four features.



Fig 4.4 Distribution of each activity class in the dataset

The model's architecture included an LSTM layer featuring 128 filters, a dropout layer, and a rectified linear unit (ReLU) activation function. The dropout layer randomly sets the weights of 50% of input units to zero, which simplifies the network. Finally, a fully connected layer with 5 units and a soft-max activation function was added. During training, the Adam optimizer was employed to minimize the loss function, utilizing the default values for β_1 , β_2 , and ϵ as they have been found to be effective for a variety of neural network architectures. The Keras Python library was utilized to construct and train the neural network. Figure 4.5 portrays the architecture utilized in all three models.



A sequential model, a linear stack of layers is used.

1. Reshaping the input to 50 x 4, with 50 data points and 4 features
2. LSTM layer with 128 units.
3. A dropout layer to avoid overfitting.
4. A dense fully connected layer to interpret the features extracted by the LSTM hidden layer
4. Finally, an output layer with SoftMax activation returns an array of size 5. One unit representing each activity.

Fig 4.5 The long short-term memory recurrent neural network architecture used for the model trained on sensor data integrated with FSR values.

4.3 Results

The results of the model are presented in the form of a confusion matrix and performance metrics for each activity. The metrics are recall, precision, and specificity. Recall, also known as sensitivity, is the ability to correctly identify the right activity while precision is a measure of the proportion of correctly predicted activities. Specificity is measured for every activity and is the ability of a model to correctly classify all other activities as negative. The model achieved an overall accuracy of 89%. The confusion matrix and performance metrics of this model are presented below.

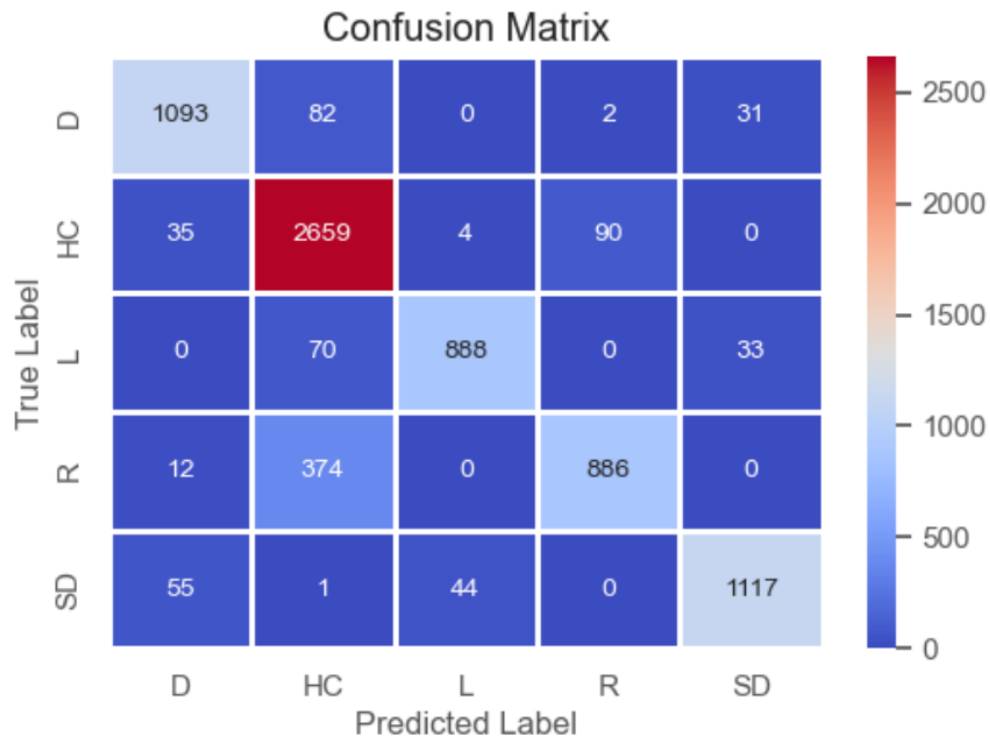


Fig 4.6 Confusion matrix from the model trained on data with FSR values as a correlating feature.

Table 4.1 Activity - specific performance metrics for the model trained on data with FSR values as a correlating feature.

| Activity | Recall/Sensitivity | Specificity | Precision |
|--------------------------------|--------------------|-------------|-----------|
| D (Lowering the bottle) | 0.90 | 0.98 | 0.91 |
| HC (Open/Close cap) | 0.95 | 0.88 | 0.83 |
| L (Lifting the bottle) | 0.90 | 0.99 | 0.95 |
| R (Bottle at rest) | 0.70 | 0.98 | 0.91 |
| SD (Squeeze the bottle) | 0.92 | 0.98 | 0.95 |
| Overall accuracy: 89% | | | |

4.3.1 Comparing results.

A similar study performed by Dr. Omkar, focusing on the development of a human activity recognition model trained on patient handling of eye-drop bottles, achieved an overall accuracy of 87%. To identify the different activities, a convolutional neural network (CNN) was trained. The results of this model are presented in the form of a confusion matrix (figure 4.7 (50)) and performance metrics for each activity.

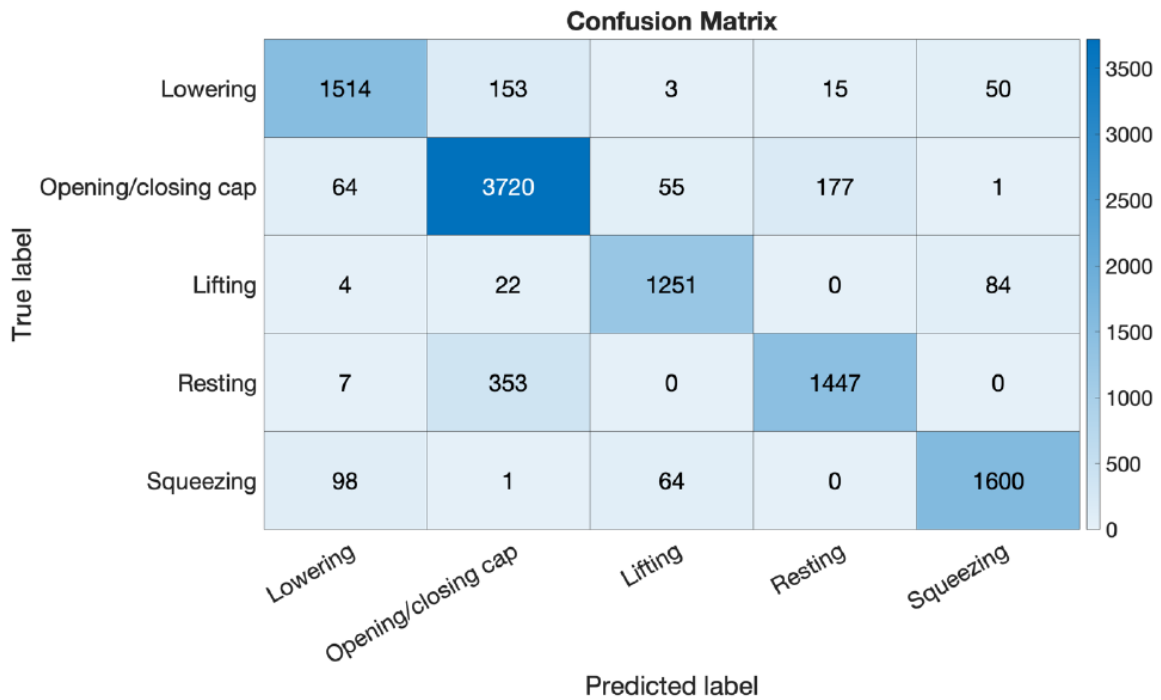


Fig 4.7 Confusion matrix from the CNN model

Table 4.2 Activity - specific performance metrics for the model trained on data with FSR values as a correlating feature using the CNN model.

| Activity | Recall/Sensitivity | Specificity | Precision |
|--------------------------------|--------------------|-------------|-----------|
| D (Lowering the bottle) | 0.87 | 0.98 | 0.90 |
| HC (Open/Close cap) | 0.93 | 0.92 | 0.88 |
| L (Lifting the bottle) | 0.92 | 0.99 | 0.91 |
| R (Bottle at rest) | 0.81 | 0.98 | 0.88 |
| SD (Squeeze the bottle) | 0.91 | 0.98 | 0.92 |
| Overall accuracy: 87% | | | |

Figures 4.8, 4.9 and 4.10 compare the performance metric of each activity between the LSTM and CNN model.

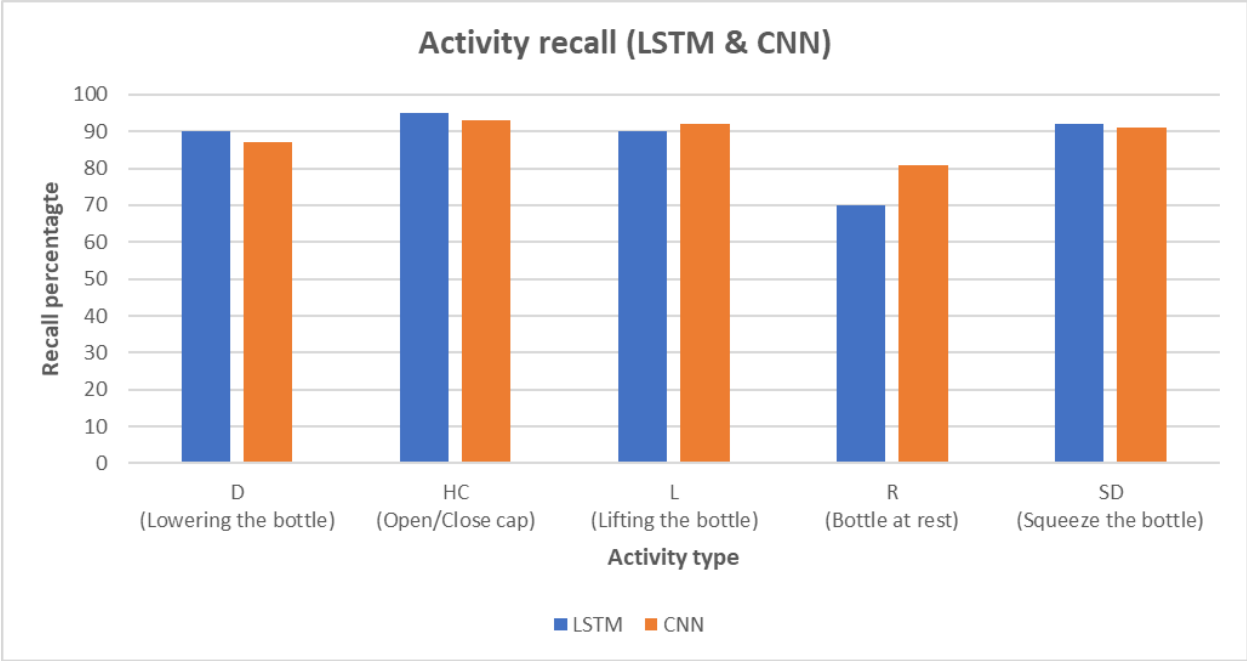


Fig 4.8 Comparing recall metrics per activity between LSTM and CNN model.

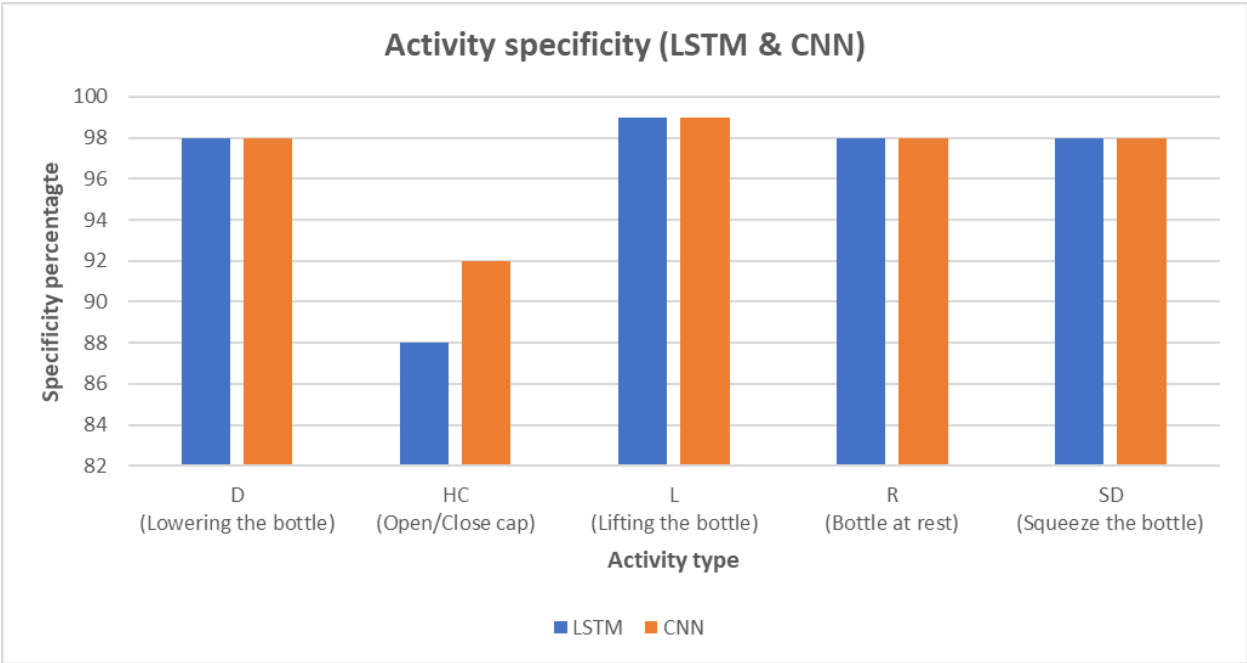


Fig 4.9 Comparing specificity metrics per activity between LSTM and CNN model.

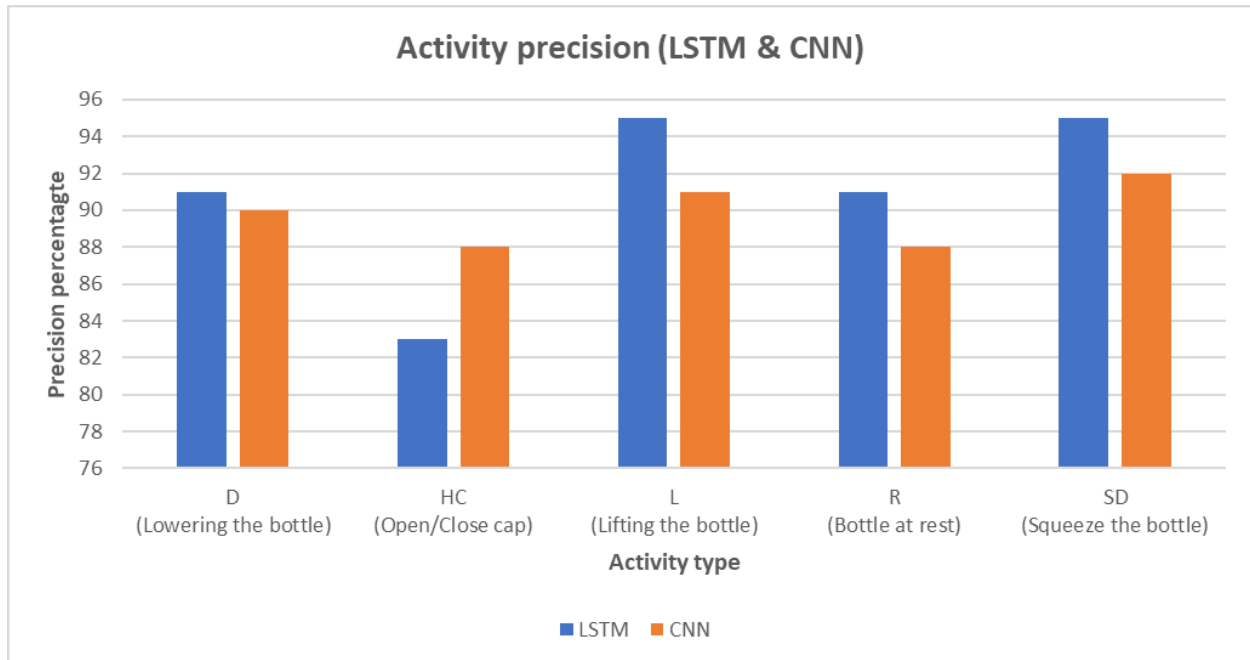


Fig 4.10 Comparing precision metrics per activity between LSTM and CNN model.

4.6 Discussion

The focus of this chapter was to develop a deep learning model that can leverage data of handling an eye-drop bottle while administering the topical medication in glaucoma patients. With chapter 2, we were able to successfully build a model that predicted all activities associated with dispensing while using a drop-delivery aid. The model developed in this chapter has been built using accelerometer data with FSR values added as a correlated feature. The need for such a model stemmed from the possible shortcomings of model 1. The model from chapter 2 was bolstered using a compliance aid called the GentleDrop™; a silicone nose-pivoted drop delivery device (NPDD) that improves accuracy in placement. Use of such a device stabilized inertial data of the dispense activity. In the absence of the NPDD the model would perform poorly because of the destabilized data. Therefore, a new model was developed.

The model achieved an overall accuracy of 89%. Ideally, the model should predict the activity of dispensing a drop with more certainty to successfully track the progress of a patient

and subsequently improve adherence to glaucoma medication. The 'resting' activity was misclassified as 'opening/closing' as seen from the confusion matrix. One possible explanation is that the variability in FSR values is affecting the performance of the model. As seen in figure 4.3 the FSR values at rest were higher than expected and could be classified as another activity. Omkar et al. suggested the use of a more complex model such as the LSTM RNN to improve the performance of the model (50), but in the absence of a higher quality of data the model still fails to perform any better. The dataset used here is limited and small; a larger dataset could improve the performance of the model. Furthermore, resolving issues such as unwieldy prototype which affects the performance of the model, fabricating an FSR that is not agnostic to the bottle dimensions and finally the data being collected at an accelerated rate which does not reflect the real-world scenario should improve the model.

A deeper look into the performance metrics per activity shows that the LSTM model achieved higher overall precision percentages. A common trend across the performance metrics is the comparatively low results for HC (open/close) activities. As seen earlier, instability in the recorded FSR values while the bottle was at rest impacts the model performance and is seen in the models recall metrics for the 'rest' activity. Though the LSTM model was able to achieve a high overall accuracy, a modification of the physical setup is required. Use of commercially available FSRs, compact setup and higher quality dataset would positively impact the performance.

All highlighted issues are a minor bump in the progression of HAR models to improve patient adherence to glaucoma medication. Integrating HAR models with patient care can provide crucial data on patient behavior and help develop unique treatment plans.

CHAPTER 5

This chapter is a summary of the important results from the research objective of this dissertation: to investigate data-based approaches to improve patient adherence to glaucoma medication and manage the disease effectively.

The intent of chapter 2 was to develop a human activity recognition (HAR) model to understand how patients interacted with eye-drop bottles used to administer glaucoma medication with the use of a drop delivery aid, GentleDrop™. The model predicted activities associated with handling an eye-drop bottle and the GentleDrop™ such as: lifting the bottle and GentleDrop™, inserting the bottle into the GentleDrop™, opening/closing the bottle, squeezing the bottle to administer a drop, lowering the bottle, separating the bottle from the GentleDrop™ and leaving them to rest. The motion of bottle and GentleDrop™ was recorded with the use of an inertial measurement unit (IMU). A long short-term memory (LSTM) recurrent neural network (RNN) was trained on the data obtained from handling the GentleDrop™ and a glaucoma eye-drop bottle. The results were positive and encouraging with overall accuracies of 86% and 88% for models trained in 8 activity classes and 7 activity classes with a combined class of lowering and closing the bottle, respectively.

With chapter 3, the aim was to tackle possible shortcomings of training a model on datasets collected from a single orientation of the inertial measurement unit (IMU). The data was transformed from a local frame of reference, the sensor frame, to a global frame of reference, the North-East-Down reference frame. Using rotation matrices and Euler angles the frame of reference was changed and a model was trained with the transformed accelerometer data added as a feature. Similar to the model in chapter 2, seven activity classes were predicted using long short term memory (LSTM) recurrent neural networks (RNN). The model was able to predict

activities with an overall accuracy of 88%. With promising results, the ability to successfully predict dispensing a drop at varying orientations improves the versatility of the model and contributes to improving glaucoma management.

With chapter 2 and 3 focused on predicting activities involved in administering an eye-drop while using a drop delivery aid such as GentleDrop™, chapter 4 dived into developing a human activity recognition model in the absence of a delivery aid. The GentleDrop™ provided stability to the process of administering a drop and largely helped the model in predicting said activities. Therefore, an FSR was integrated into the eye-drop bottle and its values added as a correlating feature. The activities involved were different: opening the bottle, lifting it to eye level, squeezing the bottle to administer a drop, lowering the bottle, closing the cap, and leaving it to rest. A LSTM recurrent neural network was trained on accelerometer and FSR data. The results were encouraging with the high overall accuracy of 89%. In comparison to other studies performed using convolutional neural networks, the LSTM model achieved higher precision percentages as well as a higher overall accuracy. In the future, these models can be used to leverage data gathered from smart eye drops used in a real-world scenario to actively improve patient adherence to their medication and allow primary care physicians to intervene at the right moment.

REFERENCES

- [1]. Quigley HA, Broman AT. The number of people with glaucoma worldwide in 2010 and 2020. *British Journal of Ophthalmology*. 2006 /03/01;90(3):262-7.
- [2]. Glaucoma [Internet]. [cited Feb 27, 2023]. Available from: <https://www.hopkinsmedicine.org/health/conditions-and-diseases/glaucoma>.
- [3]. Guo L, Moss SE, Alexander RA, Ali RR, Fitzke FW, Cordeiro MF. Retinal Ganglion Cell Apoptosis in Glaucoma Is Related to Intraocular Pressure and IOP-Induced Effects on Extracellular Matrix. *Invest Ophthalmol Vis Sci*. 2005;46(1):175-82.
- [4]. Sit AJ, John H.K. Liu. Pathophysiology of Glaucoma and Continuous Measurements of Intraocular Pressure. *Molecular & Cellular Biomechanics*. 2009;6(1):57-70.
- [5]. Agarwal R, Gupta SK, Agarwal P, Saxena R, Agrawal SS. Current concepts in the pathophysiology of glaucoma. *Indian Journal of Ophthalmology*. 2009 Jul-Aug;57(4):257.
- [6]. Kaushik S, Pandav SS, Ram J. Neuroprotection in glaucoma. *Journal of Postgraduate Medicine*. 2003 1/1;49(1):90.
- [7]. Weinreb RN, Aung T, Medeiros FA. The Pathophysiology and Treatment of Glaucoma: A Review. *JAMA*. 2014;311(18):1901-11.
- [8]. Gupta N, Weinreb RN. New definitions of glaucoma. *Curr Opin Ophthalmol*. 1997 - 04;8(2):38-41.
- [9]. Tielsch JM, Katz J, Singh K, Quigley HA, Gottsch JD, Javitt J, et al. A Population-based Evaluation of Glaucoma Screening: The Baltimore Eye Survey. *Am J Epidemiol*. 1991;134(10):1102-10.
- [10]. KLEIN BEK, KLEIN R, SPONSEL WE, FRANKE T, CANTOR LB, MARTONE J, et al. Prevalence of glaucoma: the beaver dam eye study. *Ophthalmology (Rochester, Minn.)*. 1992 Oct 1;99(10):1499-504.
- [11]. Weinreb RN, Khaw PT. Primary open-angle glaucoma. *The Lancet*. 2004;363(9422):1711-20.
- [12]. Crabb DP, Smith ND, Glen F, Burton R, Garway-Heath DF. How does glaucoma look?: Patient perception of visual field loss. *Ophthalmology*. 2013;120(6):1120-6.
- [13]. Gramer G, Gramer E. Stage of visual field loss and age at diagnosis in 1988 patients with different glaucomas: implications for glaucoma screening and driving ability. *Int Ophthalmol*. 2018 Apr 1;38(2):429-41.

- [14]. Epstein DL, Krug JH, Hertzmark E, Remis LL, Edelstein DJ. A Long-term Clinical Trial of Timolol Therapy Versus No Treatment in the Management of Glaucoma Suspects. *Ophthalmology* (Rochester, MN). 1989 Oct 1;96(10):1460-7.
- [15]. Kass MA, Heuer DK, Higginbotham EJ, Johnson CA, Keltner JL, Miller JP, et al. The Ocular Hypertension Treatment Study: A Randomized Trial Determines That Topical Ocular Hypotensive Medication Delays or Prevents the Onset of Primary Open-Angle Glaucoma. *Arch Ophthalmol*. 2002;120(6):701-13.
- [16]. Heijl A, Leske MC, Bengtsson B, Hyman L, Bengtsson B, Hussein M. Reduction of intraocular pressure and glaucoma progression: results from the Early Manifest Glaucoma Trial. *Arch Ophthalmol*. 2002 -10;120(10):1268-79.
- [17]. Li T, Lindsley K, Rouse B, Hong H, Shi Q, Friedman DS, et al. Comparative Effectiveness of First-Line Medications for Primary Open-Angle Glaucoma: A Systematic Review and Network Meta-analysis. *Ophthalmology* (Rochester, Minn.). 2016 Jan 1;123(1):129-40.
- [18]. Robin A, Grover DS. Compliance and adherence in glaucoma management. *Indian Journal of Ophthalmology*. 2011 Jan 1;59 Suppl(7):S93-6.
- [19]. Osterberg L, Blaschke T. Adherence to Medication. *New England Journal of Medicine*. 2005 -08-04;353(5):487-97.
- [20]. Daniel Shu Wei Ting, Pasquale LR, Peng L, Campbell JP, Lee AY, Raman R, et al. Artificial intelligence and deep learning in ophthalmology. *Br J Ophthalmol*. 2019;103(2):167.
- [21]. Abràmoff MD, Lavin PT, Birch M, Shah N, Folk JC. Pivotal trial of an autonomous AI-based diagnostic system for detection of diabetic retinopathy in primary care offices. *npj Digital Med*. 2018 -08-28;1(1):1-8.
- [22]. Devalla SK, Zhang L, Pham TH, Boote C, Strouthidis NG, Thiery AH, et al. Glaucoma management in the era of artificial intelligence. *Br J Ophthalmol*. 2020;104(3):301.
- [23]. Sanchez FG, Mansberger SL, Kung Y, Gardiner SK, Burgoyne CF, Cunningham ET, et al. Novel Eye Drop Delivery Aid Improves Outcomes and Satisfaction. *Ophthalmology. Glaucoma*. 2021 Sep 1;4(5):440-6.
- [24]. OLTHOFF CMG, SCHOUTEN JSAG, VAN DE BORNE BW, WEBERS CAB. Noncompliance with ocular hypotensive treatment in patients with glaucoma or ocular hypertension : An evidence-based review. *Ophthalmology* (Rochester, Minn.). 2005 Jun 1;112(6):953-61.
- [25]. Quigley HA, Kee Park C, Tracey PA, Pollack IP. Community screening for eye disease by laypersons: the Hoffberger program. *American journal of ophthalmology*. 2002 Mar 1;133(3):386-92.

- [26]. Tham Y, Li X, Wong TY, Quigley HA, Aung T, Cheng C. Global prevalence of glaucoma and projections of glaucoma burden through 2040: a systematic review and meta-analysis. *Ophthalmology (Rochester, Minn.)*. 2014 Nov;121(11):2081-90.
- [27]. Nordstrom BL, Friedman DS, Mozaffari E, Quigley HA, Walker AM. Persistence and Adherence With Topical Glaucoma Therapy - ScienceDirect. *American journal of ophthalmology*. 2005 Oct 1;140(4):598.e1,598.e11.
- [28]. Friedman DS, Quigley HA, Gelb L, Tan J, Margolis J, Shah SN, et al. Using Pharmacy Claims Data to Study Adherence to Glaucoma Medications: Methodology and Findings of the Glaucoma Adherence and Persistency Study (GAPS). *Invest Ophthalmol Vis Sci*. 2007;48(11):5052-7.
- [29]. Friedman, David S., MD, PhD, Okeke, Constance O., MD, MSCE, Jampel, Henry D., MD, MHS, Ying G, PhD, Plyler RJ, BA, Jiang, Yuzhen, MD, PhD, et al. Risk Factors for Poor Adherence to Eyedrops in Electronically Monitored Patients with Glaucoma. *Ophthalmology (Rochester, Minn.)*. 2009 Jun 1;116(6):1097-105.
- [30]. Tsai, James C., MD, MBA. A Comprehensive Perspective on Patient Adherence to Topical Glaucoma Therapy. *Ophthalmology (Rochester, Minn.)*. 2009 Nov 1;116(11):S30-6.
- [31]. FRIEDMAN DS, HAHN SR, GELB L, TAN J, SHAH SN, KIM EE, et al. Doctor-Patient Communication, Health-Related Beliefs, and Adherence in Glaucoma : Results from the Glaucoma Adherence and Persistency Study. *Ophthalmology (Rochester, Minn.)*. 2008 Aug;115(8):1320-7.
- [32]. HUGHES CM. Medication Non-Adherence in the Elderly: How Big is the Problem? *Drugs & Aging*. 2004 Jan 1;21(12):793-811.
- [33]. Friedman DS, Jampel HD, Congdon NG, Miller R, Quigley HA. The TRAVATAN Dosing Aid Accurately Records When Drops Are Taken. *American journal of ophthalmology*. 2007 Apr 1;143(4):699-701.
- [34]. Cronin TH, Kahook MY, Lathrop KL, Noecker RJ. Accuracy and performance of a commercially available Dosing Aid. *British Journal of Ophthalmology*. 2007 /04/01;91(4):497-9.
- [35]. Taking Steps Toward Better Compliance: A look at the impediments in the way of good compliance and how to overcome them. [Internet]. [].
- [36]. Gatwood JD, Johnson J, Jerkins B. Comparisons of Self-reported Glaucoma Medication Adherence With a New Wireless Device: A Pilot Study. *Journal of Glaucoma*. 2017 -11-01;26(11):1056-61.
- [37]. OKEKE CO, QUIGLEY HA, JAMPEL HD, YING G, PLYLER RJ, YUZHEN JIANG, et al. Adherence with Topical Glaucoma Medication Monitored Electronically : The Travatan Dosing Aid Study. *Ophthalmology (Rochester, Minn.)*. 2009 Feb 1;116(2):191-9.

- [38]. Schwartz GF. Compliance and persistency in glaucoma follow-up treatment. *Current Opinion in Ophthalmology*. 2005 April;16(2):114.
- [39]. Keras: Deep Learning for humans.
- [40]. Stisen A, Blunck H, Bhattacharya S, Prentow TS, Kj aergaard MB, Dey A, et al. Smart Devices Are Different: Assessing and Mitigating Mobile Sensing Heterogeneities for Activity Recognition. *Proceedings of the 13th ACM Conference on Embedded Networked Sensor Systems*; Seoul, South Korea. New York, NY, USA: Association for Computing Machinery; 2015.
- [41]. Thiemjarus S. A Device-Orientation Independent Method for Activity Recognition. ; 2010-06.
- [42]. Kunze K, Lukowicz P, Junker H, Tröster G. Where am I: Recognizing On-body Positions of Wearable Sensors. In: *Lecture notes in computer science*. Berlin, Heidelberg: Springer Berlin Heidelberg; 2005. p. 264-75.
- [43]. Accurate Activity Recognition Using a Mobile Phone Regardless of Device Orientation and Location [Internet]. [cited Apr 24, 2023]. Available from: <https://ieeexplore-ieee-org.prox.lib.ncsu.edu/document/5955295>.
- [44]. Torge W, Müller J. *Geodesy*. De Gruyter; 2012.
- [45]. MPU-9250 Product Specification. 1.1st ed. ; 2016.
- [46]. Titterton D, Weston JL, Weston J. *Strapdown inertial navigation technology*. IET; 2004.
- [47]. Dask DataFrame — Dask documentation.
- [48]. `numpy.array` — NumPy v1.24 Manual.
- [49]. Chung S, Lim J, Noh KJ, Kim G, Jeong H. Sensor Data Acquisition and Multimodal Sensor Fusion for Human Activity Recognition Using Deep Learning. *Sensors (Basel, Switzerland)*. 2019 Apr 10,;19(7):1716.
- [50]. KASKAR OG. Numerical Modeling to Understand the Pathophysiology of Glaucoma and Investigating Data-Driven Approaches for its Effective Management.[dissertation].